

1 Introduction

1.1 Background

Composite materials with a ceramic or metal matrix offer significant performance advantages over monolithic ceramics or metals. Structural ceramics exhibit high mechanical strength, superior temperature stability and good chemical durability. However, ceramics have low fracture toughness because of their ionic or covalent bonding. The intrinsic brittleness of ceramics limits their applications in industrial sectors. In this context, discontinuous fibers or whiskers are incorporated into ceramics in order to reinforce and toughen them. Upon application of external stress, matrix microcracking occurs followed by debonding of fibers from the matrix, and subsequent bridging of fibers across matrix cracks. These processes contribute to major energy dissipating events, thereby improving the fracture toughness of ceramics. Recently, metal-matrix composites (MMCs) have become increasingly used for applications in the automotive and aerospace industries because of their high specific modulus, strength and thermal stability. MMCs are reinforced with relatively large volume fractions of continuous fiber, discontinuous fibers, whiskers or particulates. The incorporation of ceramic reinforcement into the metal matrix generally leads to enhancement of strength and stiffness at the expense of fracture toughness. Further enhancement in mechanical strength of composites can be achieved by using nanostructured ceramic particles [1–4].

With tougher environmental regulations and increasing fuel costs, weight reduction in composites has become an important issue in the design of composite materials. The need for advanced composite materials having enhanced functional properties and performance characteristics is ever increasing in industrial sectors. Since their discovery by Iijima in 1991 [5], carbon nanotubes (CNTs) with high aspect ratio, large surface area, low density as well as excellent mechanical, electrical and thermal properties have attracted scientific and technological interests globally. These properties have inspired interest in using CNTs as reinforcing materials for polymer-, metal- or ceramic-matrix composites to obtain light-weight structural materials with enhanced mechanical, electrical and thermal properties [6–8]. Composite materials with at least one of their constituent phases being less than

100 nm are commonly termed “nanocomposites”. Remarkable improvements in the mechanical and physical properties of polymer-, metal- and ceramic nanocomposites can be achieved by adding very low loading levels of nanotubes. So far, extensive studies have been conducted on the synthesis, structure and property of CNT-reinforced polymers. The effects of CNT additions on the structure and property of metals and ceramics have received increasing attention recently.

1.2 Types of Carbon Nanotubes

Hybridization of the carbon atomic orbital in the forms of sp , sp^2 and sp^3 produces different structural forms or allotropes [9] (Figure 1.1). The sp -hybridization (carbyne) corresponds to a linear chain-like arrangement of atomic orbital. Carbon in the form of diamond exhibits a sp^3 -type tetrahedral covalent bonding. Each carbon atom is linked to four others at the corners of a tetrahedron via covalent bonding. This structure accounts for the extremely high hardness and density of diamond. The bonding in graphite is sp^2 , with each atom joined to three neighbors in a trigonal

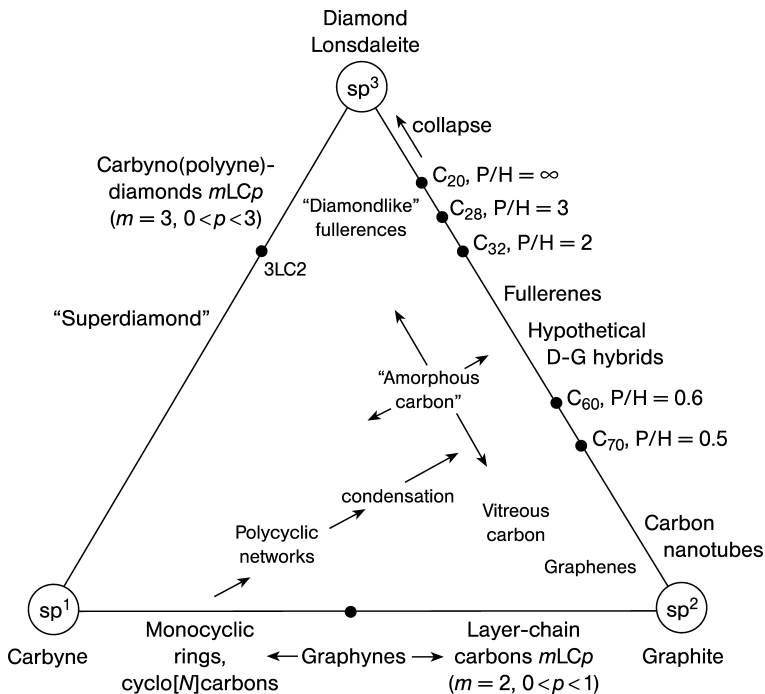


Figure 1.1 Tentative carbon allotropy diagram based on valence bond hybridization. P/H corresponds to the ratio of pentagonal/hexagonal rings. Reproduced with permission from [9]. Copyright © (1997) Elsevier.

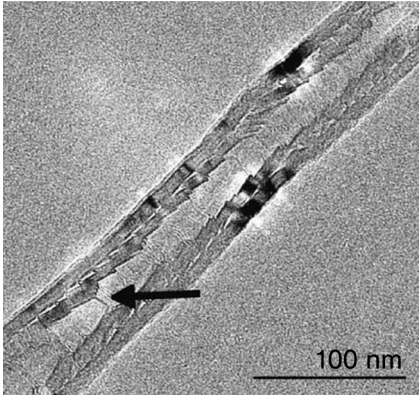


Figure 1.2 Transmission electron micrograph of the double-layer carbon nanofiber having a truncated cone structure (indicated by an arrow). Reproduced with permission from [13]. Copyright © (2006) Springer Verlag.

planar arrangement to form sheets of hexagonal rings. Individual sheets are bonded to one another by weak van der Waals forces. As a result, graphite is soft, and displays electrical conductive and lubricating characteristics. All other carbon forms are classified into intermediate or transitional forms in which the degree of hybridization of carbon atoms can be expressed as sp^n ($1 < n < 3$, $n \neq 2$). These include fullerenes, carbon onions and carbon nanotubes [9]. Fullerene is made up of 60 carbon atoms arranged in a spherical net with 20 hexagonal faces and 12 pentagonal faces, forming a truncated icosahedral structure [10, 11].

Carbon nanotubes are formed by rolling graphene sheets of hexagonal carbon rings into hollow cylinders. Single-walled carbon nanotubes (SWNT) are composed of a single graphene cylinder with a diameter in the range of 0.4–3 nm and capped at both ends by a hemisphere of fullerene. The length of nanotubes is in the range of several hundred micrometers to millimeters. These characteristics make the nanotubes exhibit very large aspect ratios. The strong van der Waals attractions that exist between the surfaces of SWNTs allow them to assemble into “ropes” in most cases. Nanotube ropes may have a diameter of 10–20 nm and a length of 100 μm or above. Multi-walled carbon nanotubes (MWNT) comprise 2 to 50 coaxial cylinders with an interlayer spacing of 0.34 nm. The diameter of MWNTs generally ranges from 4 to 30 nm [12]. The arrangement of concentric graphene cylinders in MWNTs is somewhat similar to that of Russian doll. In contrast, a nanofiber consists of stacked curved graphite layers that form cones or cups (Figure 1.2). The stacked cone and cup structures are commonly referred to as “herringbone” and “bamboo” nanofibers [13, 14].

Conceptually, the graphene sheets can be rolled into different structures, that is, zig-zag, armchair and chiral. Accordingly, the nanotube structure can be described by a chiral vector (\vec{C}_h) defined by the following equation:

$$\vec{C}_h = n\vec{a}_1 + m\vec{a}_2 \quad (1.1)$$

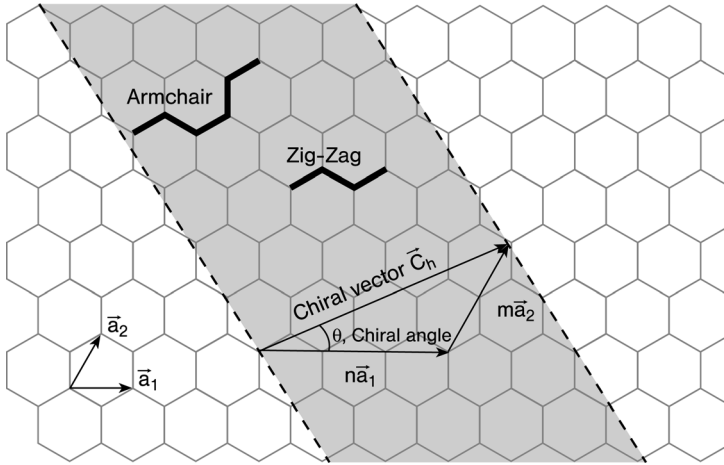


Figure 1.3 Schematic diagram showing chiral vector and chiral angle in a rolled graphite sheet with a periodic hexagonal structure. Reproduced with permission from [15]. Copyright © (2001) Elsevier.

where \vec{a}_1 and \vec{a}_2 are unit vectors in a two-dimensional hexagonal lattice, and n and m are integers. Thus, the structure of any nanotube can be expressed by the two integers n , m and chiral angle, θ (Figure 1.3). When $n = m$ and $\theta = 30^\circ$, an armchair structure is produced. Zig-zag nanotubes can be formed when m or $n = 0$ and $\theta = 0^\circ$ while chiral nanotubes are formed for any other values of n and m , having θ between 0° and 30° [15]. Mathematically, the nanotube diameter can be written as [16]:

$$d = \frac{a\sqrt{m^2 + n^2 + nm}}{\pi} \quad (1.2)$$

where a is the lattice constant in the graphene sheet, and $a = \sqrt{3}a_{C-C}$; a_{C-C} is the carbon-carbon distance (1.421 Å). The chiral angle, θ , is given by:

$$\tan \theta = \frac{\sqrt{3}m}{2n + m} \quad (1.3)$$

The electrical properties of CNTs vary from metallic to semiconducting, depending on the chirality and diameter of the nanotubes.

The demand for inexpensive carbon-based reinforcement materials is raising new challenges for materials scientists, chemists and physicists. In the past decade, vapor grown carbon nanofibers (VGCFs) with diameters ranging from 50 to 200 nm have been synthesized [17]. They are less crystalline with a stacked cone or cup structure, while maintaining acceptable mechanical and physical properties. Compared with SWNTs and MWNTs, VGCFs are available at a much lower cost because they can be mass-produced catalytically using gaseous hydrocarbons under relatively controlled conditions. VGCFs have large potential to override the cost barrier that has prevented widespread application of CNTs as reinforcing materials in industries.

1.3

Synthesis of Carbon Nanotubes

1.3.1

Electric Arc Discharge

Vaporization of carbon from solid graphite sources into a gas phase can be achieved by using electric arc discharge, laser and solar energy. Solar energy is rarely used as the vaporizing source for graphite, because it requires the use of a tailor-made furnace to concentrate an intense solar beam for vaporizing graphite target and metal catalysts in an inert atmosphere [18]. In contrast, the electric arc discharge technique is the simplest and less expensive method for fabricating CNTs. In the process, an electric (d.c.) arc is formed between two high purity graphite electrodes under the application of a larger current in an inert atmosphere (helium or argon). The high temperature generated by the arc causes vaporization of carbon atoms from anode into a plasma. The carbon vapor then condenses and deposits on the cathode to form a cylinder with a hard outer shell consisting of fused material and a softer fibrous core containing nanotubes and other carbon nanoparticles [19]. The high reaction temperature promotes formation of CNTs with a higher degree of crystallinity.

The growth mechanism of catalyst-free MWNTs is not exactly known. The nucleation stage may include the formation of C_2 precursor and its subsequent incorporation into the primary graphene structure. On the basis of transmission electron microscopy (TEM) observations, Iijima and coworkers proposed the “open-end” growth mechanism in which carbon atoms are added at the open ends of the tubes and the growing ends remains open during growth. The thickening of the tube occurs by the island growth of graphite basal planes on existing tube surfaces. Tube growth terminates when the conditions are unsuitable for the growth [20, 21]. Generally, the quality and yield of nanotubes depend on the processing conditions employed, such as efficient cooling of the cathode, the gap between electrodes, reaction chamber pressure, uniformity of the plasma arc, plasma temperature, and so on [22].

Conventional electric arc discharge generally generates unstable plasma because it induces an inhomogeneity of electric field distribution and a discontinuity of the current flow. Lee *et al.* introduced the so-called plasma rotating arc discharge technique in which the graphite anode is rotated at a high velocity of $10^4 \text{ rev min}^{-1}$ [23]. Figure 1.4 shows a schematic diagram of the apparatus. The centrifugal force caused by the rotation generates the turbulence and accelerates the carbon vapor perpendicular to the anode. The yield of the nanotubes can be monitored by changing the rotation speed. Moreover, the rotation distributes the micro discharge uniformly and generates a stable plasma with high temperatures. This enhances anode vaporization, thereby increasing carbon vapor density of nanotubes significantly. Such a technique may offer the possibility of producing nanotubes on the large scale.

Another mass production route of MWNTs can be made possible by generating electric arc discharges in liquid nitrogen [24], as shown in Figure 1.5. Liquid nitrogen prevents the electrode from contamination during arc discharge. The content of

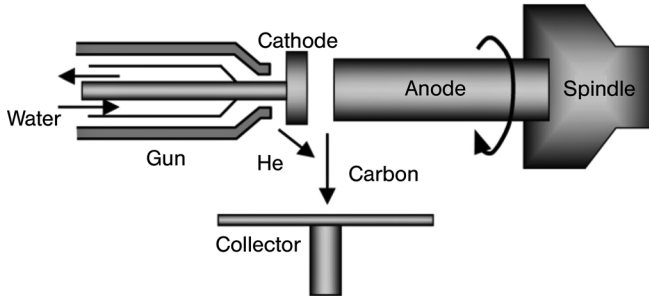


Figure 1.4 Schematic diagram of plasma rotating electrode process system. Reproduced with permission from [23]. Copyright © (2003) Elsevier.

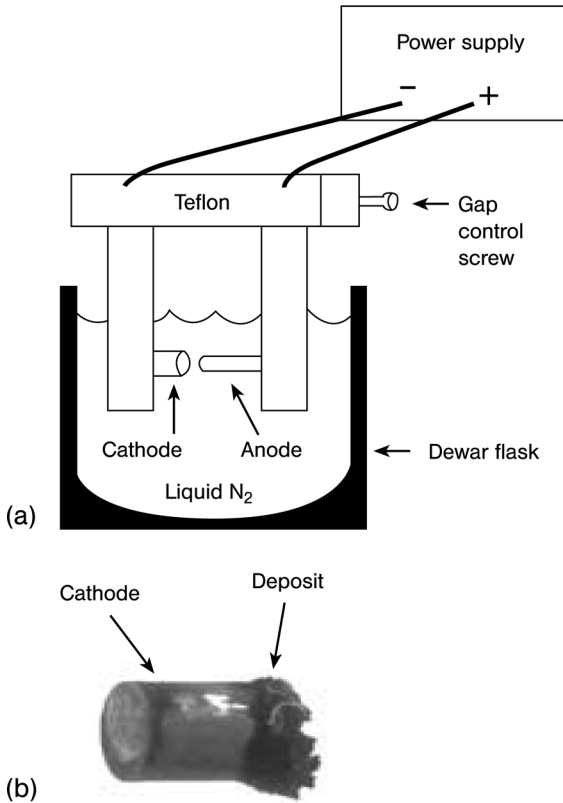


Figure 1.5 (a) Schematic drawing of the arc discharge apparatus and (b) side image of the MWNTs rich material deposited on the cathode. Reproduced with permission from [24]. Copyright © (2003) Springer Verlag.

MWNTs can be as high as 70% of the reaction product. Auger electron spectroscopic analysis reveals that nitrogen is not incorporated in the MWNTs. This technique is considered an economical route for large scale synthesis of high crystalline MWNTs as liquid nitrogen replaces expensive inert gas and cooling system for the cathode.

It is worth noting that SWNTs can only be synthesized through the arc discharge process in the presence of metal catalysts. Typical catalysts include transition metals, for example, Fe, Co and Ni, rare earths such as Y and Gd, and platinum group metals such as Rh, Ru and Pt [25–32]. In this respect, the graphite anode is doped with such metal catalysts. The synthesized nanotubes generally possess an average diameter of 1–2 nm and tangle together to form bundles in the soot, web and string-like structures. The as-grown SWNTs exhibit a high degree of crystallinity as a result of the high temperature of the arc plasma [30]. However, SWNTs contain a lot of metal catalyst and amorphous carbon, and must be purified to remove them. The yield of SWNTs produced from electric arc discharge is relatively low. The diameter and yield of SWNTs can be controlled by using a mixed gaseous atmosphere such as inert–inert or inert–hydrogen mixture [29, 30], and a mixture of metal catalyst particles [28, 32].

1.3.2

Laser Ablation

Laser ablation involves the generation of carbon vapor species from graphite target using high energy laser beams followed by the condensation of such species. The distinct advantages of laser ablation include ease of operation and production of high quality product, because it allows better control over processing parameters. The disadvantages are high cost of the laser Source and low yield of nanotubes produced.

Laser beams are coherent and intense with the capability of attaining very fast rates of vaporization of target materials. In the process, graphite target is placed inside a quartz tube surrounded by a furnace operated at 1200 °C under an inert atmosphere. The target is irradiated with a laser beam, forming hot carbon vapor species (e.g. C₃, C₂ and C). These species are swept by the flowing gas from the high-temperature zone to a conical copper collector located at the exit end of the furnace [33, 34]. Pulsed laser beam with wavelengths in infrared and visible (CO₂, Nd:YAG) or ultravioletUV (excimer) range can be used to vaporize a graphite target. This is commonly referred to as “pulsed laser vaporization” (PLV) technique [35–40]. Moreover, CO₂ and Nd:YAG lasers operated in continuous wave mode have been also reported to produce nanotubes [41–43].

SWNTs can also be produced by laser ablation but require metal catalysts as in the case of electric arc discharge. Figure 1.6 shows a TEM image of deposits formed by the laser (XeCl excimer) ablation of a graphite target containing 1.2% Ni and 1.2% Co [42]. Bimetal catalysts are believed to synthesize SWNTs more effectively than monometal catalysts [33, 36]. From Figure 1.6, SWNTs having a narrow diameter distribution (average diameter of about 1.5 nm) tend to tangle with each other to form bundles or ropes with a thickness of about 20 nm. Their surfaces are coated with amorphous carbon. Metal nanoparticles catalysts with the size of few to 10 nm can be

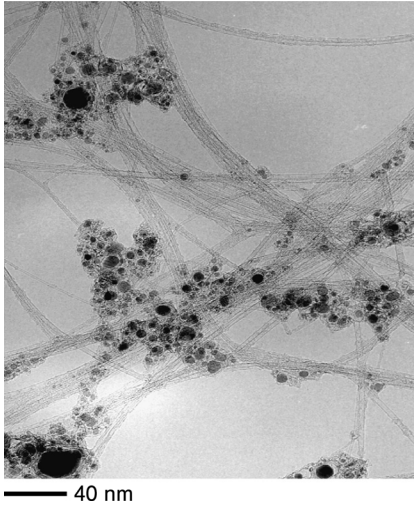


Figure 1.6 Transmission electron micrograph of a weblike deposit formed by laser ablation of a graphite target containing 1.2% Ni and 1.2%Co. The metal catalysts appeared as dark spots in the micrograph. Reproduced with permission from [40]. Copyright © (2007) Elsevier.

readily seen in the micrograph. The diameter and yield of SWNTs are strongly dependent on processing parameters such as furnace temperature, chamber pressure, laser properties (energy, wavelength, pulse duration and repetition rate) and composition of target material. The diameter of SWNTs produced by pulsed Nd:YAG laser can be tuned to smaller sizes by reducing the furnace temperature from 1200 °C down to a threshold temperature of 850 °C [35]. Using UV laser irradiation, SWNTs can be synthesized at a lower furnace temperature of 550 °C, which is much lower than the threshold temperature of 850 °C by using Nd:YAG laser [37]. Recently, Elkund *et al.* employed ultrafast (subpicosecond) laser pulses for large-scale synthesis of SWNTs at a rate of $\sim 1.5 \text{ g h}^{-1}$ [44].

To achieve controlled growth of the SWNTs, a fundamental understanding of their growth mechanism is of particular importance. The basic growth mechanism of SWNTs synthesized by physical vapor deposition (PVD) techniques is still poorly understood. The vapor–liquid–solid (VLS) mechanism is widely used to describe the catalytic formation of nanotubes via PVD [44, 45] and chemical vapor deposition (CVD) techniques [46, 47]. This model was originally proposed by Wagner and Willis to explain the formation of Si whiskers in 1964 [48]. The whiskers were grown by heating a Si substrate containing Au metal particles in a mixture of SiCl_4 and H_2 atmosphere. An Au–Si liquid droplet was formed on the surface of the Si substrate, acting as a preferred sink for arriving Si atoms. With continued incorporation of silicon atoms into the liquid droplets, the liquid droplet became saturated. Once the liquid droplet was saturated, growth occurred at the solid–liquid interface by precipitation of Si from the droplet. Wu and Yang [49] then observed direct formation

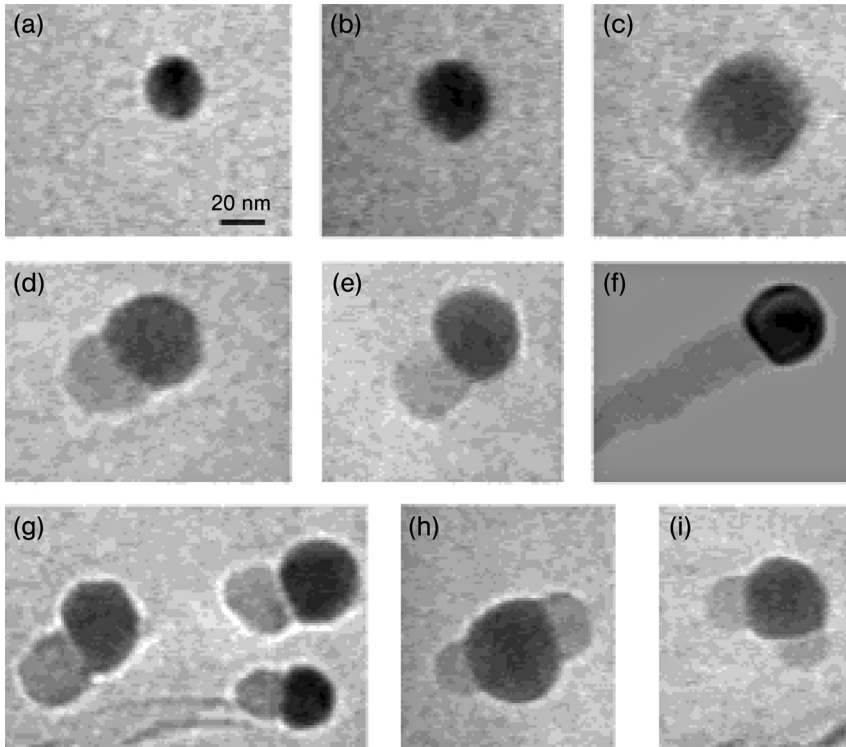


Figure 1.7 *In situ* TEM images recorded during the process of nanowire growth. (a) Au nanoclusters in solid state at 500 °C; (b) alloying initiates at 800 °C, at this stage Au exists in mostly solid state; (c) liquid Au/Ge alloy; (d) the nucleation of Ge nanocrystal on the alloy surface; (e) Ge nanocrystal elongates with further Ge condensation and eventually a wire forms (f); (g) several other examples of Ge nanowire nucleation; (h), (i) TEM images showing two nucleation events on single alloy droplet. Reproduced with permission from [49]. Copyright © (2001) The American Chemical Society.

of Ge nanowire from an Au–Ge liquid droplet using *in situ* TEM (Figure 1.7). Au nanoclusters and carbon-coated Ge microparticles were dispersed on TEM grids, followed by *in situ* heating up to 900 °C. Au nanoclusters remain in the solid state up to 900 °C in the absence of Ge vapor condensation. With increasing amount of Ge vapor condensation, Ge and Au form an eutectic Au–Ge alloy. The formation and growth of Ge nanowire is explained on the basis of VLS mechanism. Figure 1.8 shows schematic diagrams of the nucleation and growth of Ge nanowire from the eutectic Au–Ge liquid alloy.

1.3.3

Chemical Vapor Deposition

The CVD process involves chemical reactions of volatile gaseous reactants on a heated sample surface, resulting in the deposition of stable solid products on

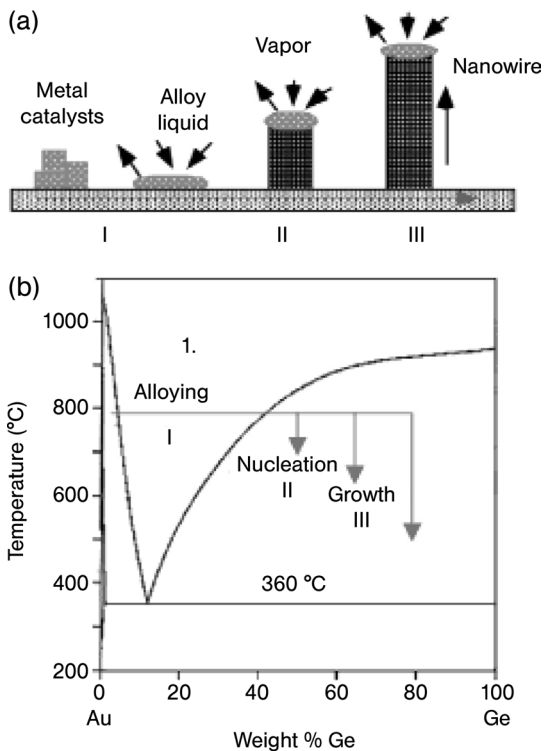


Figure 1.8 (a) Schematic illustration of vapor–liquid–solid nanowire growth mechanism including three stages: (I) alloying, (II) nucleation, and (III) axial growth. The three stages are projected onto the conventional Au–Ge binary phase diagram (b) to show the compositional and phase evolution during the nanowire growth process. Reproduced with permission from [49]. Copyright © (2001) The American Chemical Society.

the substrate. It differs distinctly from PVD techniques that involve no chemical reactions during deposition. CVD has found widespread industrial applications for the deposition of thin films and coatings due to its simplicity, flexibility, and low cost. Moreover, CVD has the ability to produce high purity ceramic, metallic and semiconducting films at high deposition rates. CVD is a versatile and cost-effective technique for CNT synthesis because it enables the use of a feedstock of hydrocarbons in solid, liquid or gas phase and a variety of substrates, and permits the growth of nanotubes in the forms of powder, thin film or thick coating, randomly oriented or aligned tubes. The process involves the decomposition of hydrocarbon gases over supported metal catalysts at temperatures much lower than the arc discharge and laser ablation. The type of CNTs produced in CVD depends on the synthesis temperatures employed. MWNTs are generally synthesized at lower temperatures

(600–900 °C) whereas SWNTs are produced at higher temperatures (900–1200 °C). However, MWNTs prepared by CVD techniques contain more structural defects than those fabricated by the arc discharge. This implies that the structure of CVD-prepared MWNTs is far from the ideal rolled-up hexagonal carbon ring lattice.

Film formation during CVD process includes several sequential steps [50]:

- (a) transport of reacting gaseous from the gas inlet to the reaction zone;
- (b) chemical reactions in the gas phase to form new reactive species;
- (c) transport and adsorption of species on the surface;
- (d) surface diffusion of the species to growth sites;
- (e) nucleation and growth of the film;
- (f) desorption of volatile surface reaction products and transport of the reaction by-products away from the surface.

CVD can be classified into thermal and plasma-enhanced and laser-assisted processes depending upon the heating Sources used to activate the chemical reactions. The heating Sources decompose the molecules of gas reactants (e.g. methane, ethylene or acetylene) into reactive atomic carbon. The carbon then diffuses towards hot substrate that is coated with catalyst particles whose size is of nanometer scale. The catalyst can be prepared by sputtering or evaporating metal such as Fe, Ni or Co onto a substrate. This is followed by either chemical etching or thermal annealing treatment to induce a high density of catalyst particle nucleation on a substrate [46, 47]. Alternatively, metal nanoparticles can be nucleated and distributed more uniformly on a substrate by using a spin-coating method [51, 52]. The size and type of catalysts play a crucial role on the diameter, growth rate, morphology and structure of synthesized nanotubes [53, 54]. In other words, the diameter and length of CNTs can be controlled by monitoring the size of metal nanoparticles and the deposition conditions. Choi *et al.* demonstrated that the growth rate of CNTs increases with decreasing the grain size of Ni film for plasma-enhanced CVD [54]. As the size of particles decreases, the diffusion time for carbon atoms to arrive at the nucleation sites becomes shorter, thereby increasing the growth rate and density of nanotubes. The yield of nanotubes depends greatly on the properties of substrate materials. Zeolite is widely recognized as a good catalyst support because it favors formation of high yield CNTs with a narrow diameter distribution [55]. Alumina is also an excellent catalyst support because it offers a strong metal-support interaction, thereby preventing agglomeration of metal particles and offering high density of catalytic sites.

1.3.3.1 Thermal CVD

In thermal CVD, thermal energy resulting from resistance heating, r.f. heating or infrared irradiation activates the decomposition of gas reactants. The simplest case is the use of a quartz tube reactor enclosed in a high temperature furnace [48–51, 53]. In the process, the metal catalyst (Fe, Co or Ni) film is initially deposited on a substrate, which is loaded into a ceramic boat in the CVD reactor. The catalytic metal film is treated with ammonia gas at 750–950 °C to induce the formation of metal

nanoparticles on the substrate. Hydrocarbon gas is then introduced into the quartz tube reactor [48, 53].

According to the VLS model, an initial step in the CVD process involves catalytic decomposition of hydrocarbon molecules on metal nanoparticles. Carbon atoms then diffuse through the metal particles, forming a solid solution. When the solution becomes supersaturated, carbon precipitates on the surface of particles and grows into CNTs. Growth can occur either below or above the metal catalyst as carbon is precipitated from supersaturated solid solution. Both base and tip growth mechanisms have been suggested. For a strong catalyst–substrate interaction, a CNT grows up with the catalyst particle pinned at its base, favoring a base-growth phenomenon [56, 57]. In the case of a tip growth mechanism, the catalyst–substrate interaction is weak, hence the catalyst particle is lifted up by the growing nanotube such that the particle is eventually encapsulated at the tip of a nanotube [58–60]. Figure 1.9(a) and (b)

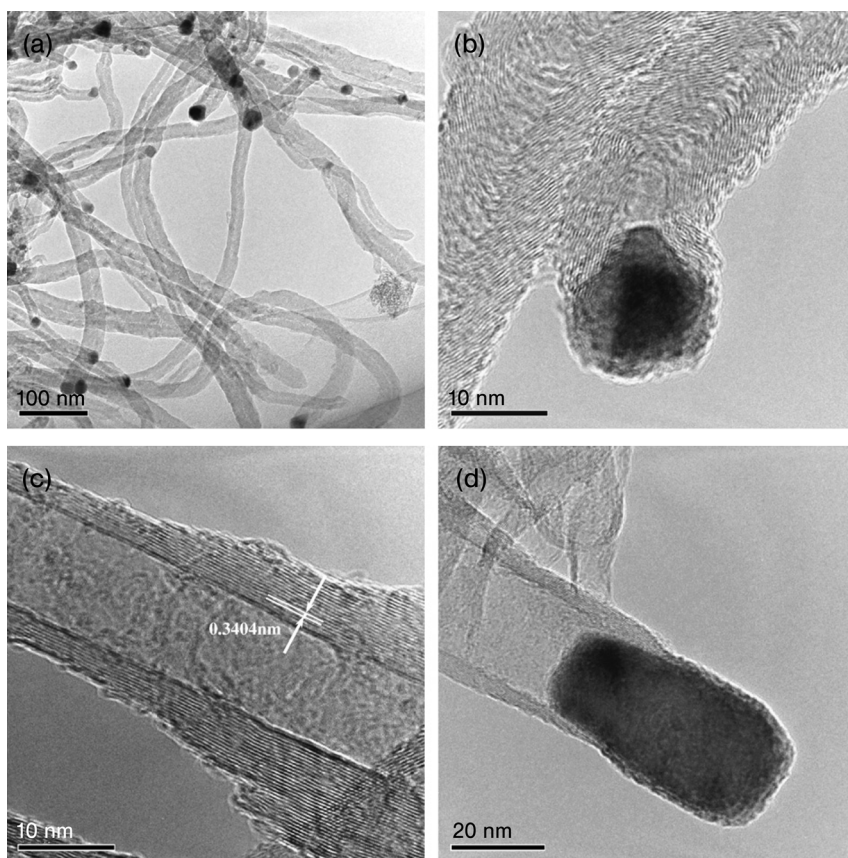


Figure 1.9 TEM images of CNTs synthesized using the catalyst with 10% nickel at 450 °C [(a) and (b)], and at 650 °C [(c) and (d)]. Reproduced with permission from [59]. Copyright © (2008) Elsevier.

show TEM images of MWNTs synthesized from thermal CVD over Ni/Al catalyst at 450 °C [59]. Long nanotubes having a diameter of about 15 nm exhibit typical coiled, spaghetti-like morphology. Some metal catalysts appear to locate at the tip of nanotubes. TEM image of MWNTs produced at 650 °C clearly shows an interlayer spacing between graphitic sheets of 0.34 nm (Figure 1.9(c)). A metal nanoparticle can be readily seen at the tip of the tube formed at 650 °C, thus indicating that a tip growth mechanism prevails in this case (Figure 1.9(d)).

Despite the fact that the thermal CVD method produces tangled and coiled nanotubes, this technique is capable of forming aligned arrays of CNTs by precisely adjusting the reaction parameters [53, 56–58, 61–63]. For practical engineering applications in the areas of field emission display and nanofillers for composites, formation of vertically aligned nanotubes is highly desirable. To achieve this, a gaseous precursor is normally diluted with hydrogen-rich gas, that is, NH_3 or H_2 . Lee *et al.* reported that NH_3 is essential for the formation of aligned nanotubes [61]. Choi *et al.* [62] demonstrated that the ammonia gas plays the role of etching amorphous carbon during the earlier stage of nucleation of nanotubes. Both synthesis by C_2H_2 after ammonia pretreatment, and synthesis by $\text{NH}_3/\text{C}_2\text{H}_2$ gas mixture without ammonia treatment favor alignment of nanotubes. Figure 1.10(a) shows the morphology of nanotubes synthesized by flowing C_2H_2 on a Ni film at 800 °C without ammonia pretreatment. Apparently, coiled nanotubes are produced without NH_3 treatment. However, well-aligned nanotubes can be formed on the Ni film with ammonia pretreatment prior to the introduction of C_2H_2 gas (Figure 1.10(b)).

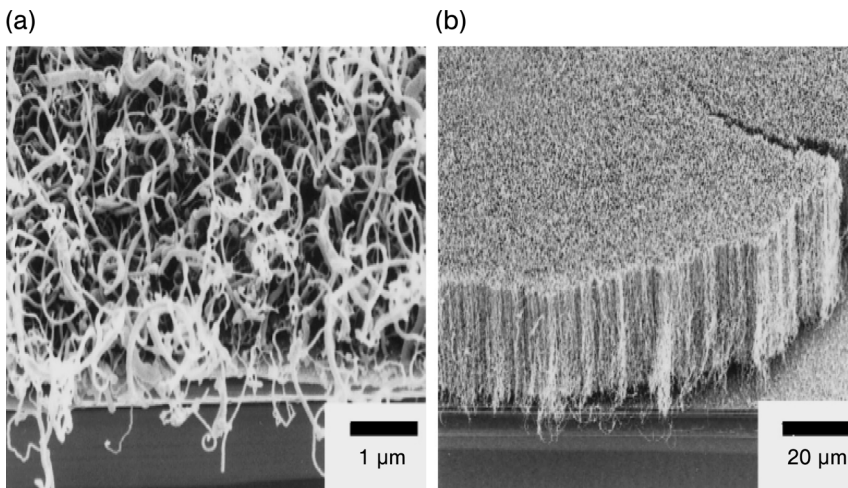


Figure 1.10 Surface morphology of CNTs synthesized by C_2H_2 gas mixture on 20 nm thick Ni films: (a) without and (b) with ammonia treatments. Reproduced with permission from [62]. Copyright © (2001) Elsevier.

1.3.3.2 Plasma-enhanced CVD

Plasma-enhanced CVD (PECVD) offers advantages over thermal CVD in terms of lower deposition temperatures and higher deposition rates. Carbon nanotubes can be produced at the relatively low temperature of 120 °C [64], and even at room temperature [65] using plasma-enhanced processes. This avoids the damage of substrates from exposure to high temperatures and allows the use of low-melting point plastics as substrate materials for nanotubes deposition. The plasma Sources used include direct current (d.c.), radio frequency (r.f.), microwave and electron cyclotron resonance microwave (ECR-MW). These Sources are capable of ionizing reacting gases, thereby generating a plasma of electrons, ions and excited radical species. In general, vertically aligned nanotubes over a large area with superior uniformity in diameter and length can be synthesized by using PECVD techniques [54, 66–70].

Among these Sources, microwave plasma is commonly used. The excitation microwave frequency (2.45 GHz) oscillates electrons that subsequently collide with hydrocarbon gases, forming a variety of C_xH_y radicals and ions. During plasma-enhanced deposition, hydrocarbon feedstock is generally diluted with other gases such as hydrogen, nitrogen and oxygen. Hydrogen or ammonia in hydrocarbon Sources inhibit the formation of amorphous carbons and enhance the surface diffusion of carbon. This facilitates formation of vertically aligned nanotubes. By regulating the types of catalyst, microwave power and the composition ratios of gas precursor, helix-shaped and spring-like MWNTs have been produced [71].

1.3.3.3 Laser assisted CVD

Laser assisted CVD (LCVD) is a versatile process capable of depositing various kinds of materials. In the process, a laser (CO_2) is used to locally heat a small spot on the substrate surface to the temperature required for deposition. Chemical vapor deposition then occurs at the gas–substrate interface. As the spot temperature increases and the reaction proceeds, a fiber nucleates at the laser spot and grows along the direction of laser beam [72]. LCVD generally has deposition rates several orders of magnitude higher than conventional CVD, thus offering the possibility to scale-up production of CNTs. Focused laser radiation permits growth of locally defined nanotube films. Rohmund *et al.* reported that films of vertically aligned MWNTs of extremely high packing density can be produced using LCVD under conditions of low hydrocarbon concentration [73]. The use of LCVD for producing nanotubes is still in the earlier development stage. Compared with PECVD, only few studies have been conducted on the synthesis of CNTs using LCVD [50, 73, 74].

1.3.3.4 Vapor Phase Growth

This refers to a synthetic process for CNTs in which hydrocarbon gas and metal catalyst particles are directly fed into a reaction chamber without using a substrate. VGCFs can be produced in higher volumes and at lower cost from natural gas using this technique. In 1983, Tibbets developed a process for continuously growing vapor grown carbon fibers up to 12 cm long by pyrolysis of natural gas in a stainless steel tube [75]. However, the diameters of graphite fibers produced are quite large, from 5 to 1000 μm depending on the growth temperature and gas flow rate.

Since then, large efforts have been spent to grow carbon fibers with diameters in the nanometer range (50–200 nm) in the vapor phase by catalytic decomposition of hydrocarbons [17, 76]. Currently, Applied Sciences Inc (ASI, Cedarville, Ohio, USA) produces VGCFs denoted as Pyrograf III of different types, namely PR-1, PR-11, PR-19 and PR-24 [77, 78]. The PR-1, PR-11, and PR-19 nanofibers are 100–200 nm in diameter and 30–100 μm in length. The PR-24 fibers are 60–150 nm in length and 30–100 μm long [77]. Pyrograf III fibers find widespread application as reinforcement materials for polymer composites [6]. In Europe, VGCFs are also commercially available from Electrovac Company [79, 80]. These nanofibers include ENF100 AA (diameter of 80–150 nm), HTF110FF (diameter of 70–150 nm) and HTF150FF (diameter of 100–200 nm); these fibers are longer than 20 μm .

Satishkumar *et al.* [81] and Jang *et al.* [82] synthesized CNTs by pyrolysis of iron pentacarbonyl $[\text{Fe}(\text{CO})_5]$ with methane, acetylene or butane. Ferrocene with a sublimation temperature of $\sim 140^\circ\text{C}$ is widely recognized to be an excellent precursor for forming Fe catalyst particles. Figure 1.11 is a schematic diagram showing a typical pyrolysis apparatus for the synthesis of CNTs. Ferrocene is placed in the first furnace heated to 350°C under flowing argon. The ferrocene vapor is carried by the argon gas into the second furnace maintained at 1100°C . Hydrocarbon gas is finally introduced into the pyrolysis zone of the second furnace. The pyrolysis of ferrocene–hydrocarbon mixture yields iron nanoparticles. After the reaction, carbon deposits are accumulated at the wall of a quartz tube near the inlet end of the second furnace. Rohmund *et al.* used a single-step, single furnace for the catalytic decomposition of C_2H_2 by ferrocene [83]. In some cases, MWNTs can be produced by pyrolyzing homogeneously dispersed aerosols generated from a solution containing both the hydrocarbon source (xylene or benzene) and ferrocene [84]. Andrews *et al.* reported that large quantities of vertically aligned MWNTs can be produced through the catalytic decomposition of a ferrocene–xylene mixture at

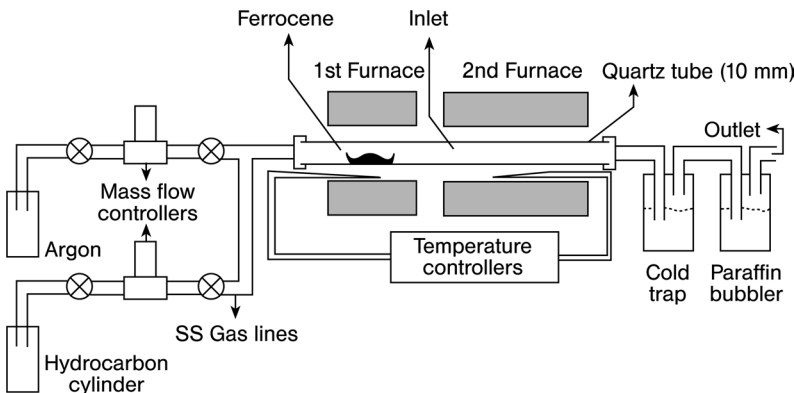


Figure 1.11 Schematic layout of a processing system designed for the synthesis of aligned CNTs by the pyrolysis of ferrocene–hydrocarbon mixtures. Reproduced with permission from [81]. Copyright © (1999) Elsevier.

~675 °C [84]. In engineering practice, a vertical tubular fluidized-bed reactor is generally used to mass-produce CNTs. Fluidization involves the transformation of solid particles into a fluid-like state through suspension in a gas or liquid. A fluidized-bed reactor allows continuous addition and removal of solid particles without stopping the operation. Wang *et al.* developed a nano-agglomerate fluidized-bed reactor in which a high yield of MWNTs of few kilograms per day can be synthesized by continuous decomposition of ethylene or propylene on the alumina supported Fe catalyst at 500–700 °C [85].

1.3.3.5 Carbon Monoxide Disproportionation

In 1999, Smalley's research group at Rice University developed the so-called high pressure CO disproportionation (HiPCo) process that can be scaled up to industry level for the synthesis of SWNTs [86]. SWNTs are synthesized in the gas phase in a flow reactor at high pressures (1–10 atm) and temperatures (800–1200 °C) using carbon monoxide as the carbon feedstock and gaseous iron pentacarbonyl as the catalyst precursor. Solid carbon is produced by CO disproportionation that occurs catalytically on the surface of iron particles via the following reaction:



Smalley demonstrated that metal clusters initially form by aggregation of iron atoms from the decomposition of iron pentacarbonyl. Clusters grow by collision with additional metal atoms and other clusters, leading to the formation of amorphous carbon free SWNT with a diameter as small as 0.7 nm [86].

In another study, Smalley and coworkers synthesized SWNTs by disproportionation of carbon dioxide on solid Mo metal nanoparticles at 1200 °C [87]. TEM image reveals that the metal nanoparticles are attached to the tips of nanotubes with diameters ranging from 1 to 5 nm. Using a similar approach, researchers at the University of Oklahoma also employed the CO disproportionation process to synthesize SWNTs in a tubular fluidized-bed reactor at lower temperatures of 700–950 °C using silica supported Co–Mo catalysts. They called this synthesis route as the CoMoCat process [88–90]. The bimetallic Co–Mo catalysts suppress formation of the MWNTs but promote SWNTs at lower temperatures. In this method, interactions between Mo oxides and Co stabilize the Co species from segregation through high-temperature sintering. The extent of interaction depends on the Co: Mo ratio in the catalyst [89]. With exposure to CO, the Mo oxide is converted to Mo carbide, and Co is reduced from the oxide state to metallic Co clusters. Carbon accumulates on such clusters through CO disproportionation, leading to the formation of SWNTs. The diameter of SWNTs can be controlled by altering processing conditions such as operating temperature and processing time. However, such synthesized SWNTs contain various impurities such as silica support and the Co and Mo species. Therefore, a further purification process is needed. Despite the improvements that have been achieved in the production of SWNTs, the price and yield of nanotubes are still far from the needs of the industry. Thus, developing a cost-effective technique for producing high yield SWNTs still remains a big challenge for materials scientists.

1.3.4

Patent Processes

Carbon nanotubes with unique, remarkable physical and mechanical characteristics are attractive materials for advanced engineering applications. Scientists from research laboratories worldwide have developed novel technical processes for the synthesis of nanotubes. Table 1.1 lists the patent processes approved by the United States Patent and Trademark Office recently for the synthesis of CNTs.

US Patent 7329398 discloses a process for the production of CNTs or VGCFs by suspending metal catalyst nanoparticles in a gaseous phase [91]. Nanoparticles are prepared in the form of a colloidal solution in the presence or absence of a surfactant. They are then introduced in a gaseous phase into a heated reactor by spraying, injection or atomization together with a carrier and/or a carbon source. Consequently, most of the problems faced by the conventional gas-phase synthetic processes can be overcome by this novel method.

US Patent 7008605 discloses a non-catalytic process for producing MWNTs by using electric arc discharge technique [92]. The electric current creates an electric arc between the carbon anode and cathode under a protective inert gas atmosphere. The arc vaporizes carbon anode, depositing carbonaceous species on the carbon cathode. The anode and cathode are cooled continuously during discharge. When the electric current is terminated, the carbonaceous residue is removed from the cathode and is purified to yield CNTs.

Table 1.1 Patent processes for production of carbon nanotubes.

Patent Number and Year	Type of Nanotubes	Fabrication Process	Inventor	Assignee
US 7329398 (2008)	MWNTs, VGCF	Vapor phase growth	Kim, Y.N.	KH Chemicals Co. (Korea)
US 7008605 (2006)	MWNTs	Electric arc discharge	Benavides, J.M.	NASA (USA)
US 7094385 (2006)	MWNTs	CVD	Beguin; F., Delpeux; S., Szostak; K.	CNRS (Paris, France)
US 7087207 (2006)	Oriented SWNTs	Laser ablation followed by oxidation and alignment in an electric field	Smalley, R. E., Colbert D.T., Dai, H., Liu, J.; Rinzler, A.G.; Hafner, J.H.; Smith, K., Guo, T., Nikolaev, P., Thess. A.	Rice University (USA)
US 6962892 (2005)	SWNTs	CO disproportionation	Resasco, D.E, Kitiyanan, B., Harwell, J.H., Alvarez, W.E	University of Oklahoma (USA)
US 6994907 (2006)	SWNTs	CO disproportionation	Resasco, D.E, Kitiyanan, B., Harwell, J.H., Alvarez, W.E	University of Oklahoma (USA)

US Patent 7094385 discloses a process for the selective mass production of MWNTs from the decomposition of acetylene diluted with nitrogen on a $\text{Co}_x\text{Mg}_{(1-x)}\text{O}$ solid solution at 500–900 °C [93]. Acetylene is a less expensive source of carbon and easy to use due to its low decomposition temperature, of 500 °C. The process comprises a catalytic step consisting of the formation of nascent hydrogen *in situ* by acetylene decomposition such that CoO is progressively reduced to Co nanometric clusters:



where $\langle \text{Co} \rangle$ represents the Co particles supported on the oxide.

US Patent 7087207 discloses the use of a purified bucky paper of SWNTs as the starting material [94]. Upon oxidation of the bucky paper at 500 °C in an atmosphere of oxygen and CO_2 , many tube and rope ends protrude from the surface of the paper. Placing the resulting bucky paper in an electric field can cause the protruding tubes and ropes of SWNTs to align in a direction perpendicular to the paper surface. These tubes tend to coalesce to form a molecular array.

For CO disproportionation, US Patent 6962892 discloses the types of catalytic metal particles used for nanotube synthesis. The bimetallic catalyst contains one metal from Group VIII including Co, Ni, Ru, Rh, Pd, Ir and Pt, and one metal from Group VIB including Cr, W, and Mo. Specific examples include Co–Cr, Co–W, Co–Mo, Ni–Cr, and so on [95]. US Patent 6994907 discloses controlled production of SWNTs based on a reliable quantitative measurement of the yield of nanotubes through the temperature-programmed oxidation technique under CO disproportionation [96]. This permits the selectivity of a particular catalyst and optimizes reaction condition for producing CNTs. The Co : Mo / SiO_2 catalysts contain Co:Mo molar ratios of 1 : 2 and 1 : 4 exhibit the highest selectivities towards SWNTs.

1.4

Purification of Carbon Nanotubes

1.4.1

Purification Processes

As mentioned above, CNTs prepared from arc discharge, laser ablation and CVD techniques contain various impurities such as amorphous carbon, fullerenes, graphite particles and metal catalysts. The presence of impurities can affect the performance of CNTs and their functional products significantly. Therefore, these impurities must be removed completely from nanotubes using appropriate methods. Typical techniques include gas-phase oxidation [97–99], liquid-phase oxidation [100–106] and physical separation [107–110].

Gas-phase and liquid-phase oxidative treatments are simple practices for removing carbonaceous byproducts and metal impurities from CNTs. In the former case, CNTs

are oxidized in air, pure oxygen or chlorine atmosphere at 500 °C [98]. However, oxidative treatment suffers the risk of burning off more than 95% of the nanotube materials [97]. Another drawback of gas-phase oxidation is inhomogeneity of the gas/solid mixture. The liquid-phase oxidative treatment can be carried out simply by dipping nanotubes into strong acids such as concentrated HNO₃, H₂SO₄, mixed 3 : 1 solution of H₂SO₄ and HNO₃, or other strong oxidizing agents such as KMnO₄, HClO₄ and H₂O₂. In some cases, a two-step (e.g. gas-phase thermal oxidation followed by dipping in acids) or multi-step purification process is adopted, to further improve the purity of CNTs [30, 111–113].

Hiura *et al.* [100] reported that oxidation of nanotubes in sulfuric or nitric acid is quite slow and weak, but a mixture of the two yields better results. The best oxidant for CNTs is KMnO₄ in acidic solution. Hernadi *et al.* [103] demonstrated that oxidation by KMnO₄ in an acidic suspension provides nanotubes free of amorphous carbon. The purification process also opens the nanotube tips on a large scale, leading to the formation of carbonyl and carboxyl functional groups at these sites. The formation of such functional groups is detrimental to the physical properties of CNTs. However, it is beneficial for fully introducing CNTs into polymers. Carbon nanotubes are known to be chemically inert and react very little with polymers. Introducing carboxyl (–COOH) groups into CNTs enhances the dispersion of CNTs in polymers because such functional groups improve the interfacial interaction between them [6]. Chen *et al.* reported that the efficiency of acid purification of CNTs can be enhanced dramatically by using microwave irradiation [104, 105]. In this technique, MWNTs are initially dispersed in a Teflon container containing 5 M nitric acid solution. The container is then placed inside a commercial microwave oven operated at 210 °C. During the purification process, nitric acid can absorb microwave energy rapidly, thereby dissolving metal particles from nanotubes effectively. More recently, Porro *et al.* combined acid and basic purification treatment on MWNTs grown by thermal CVD [106]. The purification treatment leads to an opening of the nanotube tips, with a consequent loss of metal particles encapsulated in tips.

Physical separation techniques are based on the initial suspension of SWNTs in a surfactant solution followed by size separation using filtration, centrifugation or chromatography. Bandow *et al.* reported a multiple-step filtration method to purify laser ablated SWNTs [107]. In this method, the nanotubes were first soaked in a CS₂ solution. The CS₂ insolubles were trapped in the filter, and the CS₂ solubles (e.g. fullerenes and other carbonaceous byproducts) passed through the filter. The insoluble solids caught on the filter were dispersed ultrasonically in an aqueous solution containing cationic surfactant followed by filtration. This method filters fullerenes and other carbonaceous byproducts, thus the purity of SWNTs is above 90%. The drawback of this method is apparent as it requires several experimental step procedures. Shelimov *et al.* demonstrated that a single step of ultrasonically assisted filtration can produce SWNT material with purity of >90% and yields of 30–70% [108].

Apart from high purity, length control is another important issue for successful application of CNTs in industry. As mentioned above, CNTs prepared from thermal CVD exhibit coiled morphology with lengths range from several micrometers to

Table 1.2 Comparison of the physical and chemical dispersion methods.

Method	Scale	Mechanism	Main treatment conditions
Shearing	10–100 μm	Breaking up the multi-agglomerates	24 000 r/min, 5 min
Ball milling	10–100 μm	Breaking up the multi-agglomerates	Porcelain ball (20 mm, 11 g), 3.5 h
Ultrasonic	1–300 μm	Dispersing of the single-agglomerates	59 kHz, 80 w, 10 h
Concentrated $\text{H}_2\text{SO}_4/\text{HNO}_3$	Nano-scale (individual nanotubes)	Dispersing the MWNTs by shortening their length and adding carboxylic groups	3 : 1 concentrated $\text{H}_2\text{SO}_4/\text{HNO}_3$ ultrasonicated for 0–10 h at 20–40 °C or boiled for 0.5 h at 140 °C

Reproduced with permission from [117]. Copyright © (2003) Elsevier.

millimeter scales. Entangled nanotubes tend to form large agglomerates, thus they must be dispersed or separated into shorter individual tubes prior to the incorporation into composites. The length of CNTs can be reduced through gas-phase thermal oxidation in air at 500 °C and liquid-phase acid purification [114, 115]. Cutting and dispersion of the CNTs can also be induced mechanically via ultrasonication, ball milling, and high speed shearing [116–118]. Wang *et al.* compared the effects of acid purification, ball milling, shearing, ultrasonication on the dispersion of MWNTs prepared from CVD [117]. They indicated that mechanical treatments can only break up the as-prepared agglomerates of nanotubes into smaller parts of single agglomerates. However, excellent dispersion can be achieved by dipping MWNTs in 3 : 1 $\text{H}_2\text{SO}_4/\text{HNO}_3$ acid. Their experimental conditions and results are summarized in Table 1.2. It should be noted that the cutting effect of ball milling depends on the type of mill used and milling time. Pierrad *et al.* demonstrated that ball milling is a good method to obtain short MWNTs (below 1 μm) with open tips [118]. The length of MWNTs decreases markedly with increasing milling time. Table 1.3 lists the current patent processes for the purification and cutting of CNTs.

1.4.2

Materials Characterization

After purification, materials examination techniques must be used to characterize the quality and to monitor material purity of the nanotubes qualitatively or quantitatively. A rapid discrimination of the purity level of CNTs is essential for their effective application as functional materials in electronic devices and structural materials. Analytical characterization techniques used include SEM, TEM, energy dispersed spectroscopy (EDS), Raman, X-ray diffraction (XRD), optical absorption spectroscopy and thermogravimetric analysis (TGA) [119–121]. SEM and TEM can provide morphological features of purified nanotubes. The residual metal particles present in CNTs can be identified easily by EDS attached to the electron microscopes.

Table 1.3 Patent processes for the purification of carbon nanotubes.

Patent Number and Year	Type of Nanotubes	Purification Process	Inventor	Assignee
US 7135158 (2006)	SWNTs	Multiple-step	Goto, H., Furuta, T., Fujiwara, Y., Ohashi, T.	Honda Giken Kogyo Kabushiki Kaisha (Japan)
US 7029646 (2006)	SWNTs	Fluorination	Margrave, J.L., Gu, Z., Hauge, R.H., Smalley, R.E.	Rice University (USA)
US 7115864 (2006)	SWNTs	Liquid-phase oxidation	Colbert, D.T., Dai, H., Hafner, J.H., Rinzler, A.G., Smalley, R.E., Liu, J., Smith, K.A., Guo, T., Nikolaev, P., Thess, A.	Rice University (USA)
US 6841003 (2005)	SWNTs	Plasma etching	Kang, S.G., Bae, C.	cDream Display Corporation (USA)

Electron microscopy coupled with EDS gives rise to qualitative information for purified nanotubes. In general, TEM observation is preferred because it offers high-resolution images. However, sample preparation for TEM examination is tedious and time consuming. Moreover, electron microscopic observations are mainly focused on localized regions of the samples, thus the analyzed sampling volumes are relatively small.

Raman spectroscopy is a qualitative tool for determining vibrational frequency of molecular allotropes of carbon. All carbonaceous moieties such as fullerenes, CNTs, diamond, and amorphous carbon are Raman active. The position, width and relative intensity of Raman peaks are modified according to the sp^3 and sp^2 configurations of carbon [122–124]. Raman spectra of the SWNTs are well characterized by the low frequency radial breathing mode (RBM) at $150\text{--}200\text{ cm}^{-1}$, with frequency depending on the tube diameter and the tangential mode at $1400\text{--}1700\text{ cm}^{-1}$. From the spectral analysis, a sharp G peak at $\sim 1590\text{ cm}^{-1}$ is related to the (C–C) stretching mode, and a band at $\sim 1350\text{ cm}^{-1}$ is associated with disorder-induced band (D band). Moreover, a second order mode at $2450\text{--}2650\text{ cm}^{-1}$ is assigned to the first overtone of D mode and commonly referred to as G' mode. The D-peak is forbidden in perfect graphite and only becomes active in the presence of disorder [122]. In general, the full-width at half-maximum (FWHM) intensity of the D-peak for various carbon impurities is generally much broader than that of the nanotubes. Thus, the purity level of SWNTs can be simply obtained by examining the linewidth of the D-peak [120, 123]. Alternatively, the D/G intensity ratio can be used as an indicator for the purity levels of SWNTs. In the presence of defects, a slight increase in the D-band intensity relative to the intensity of G-band is observed [125].

XRD is a powerful tool for identifying the crystal structure of metal catalysts and carbonaceous moieties. The lattice constant of these species can be determined

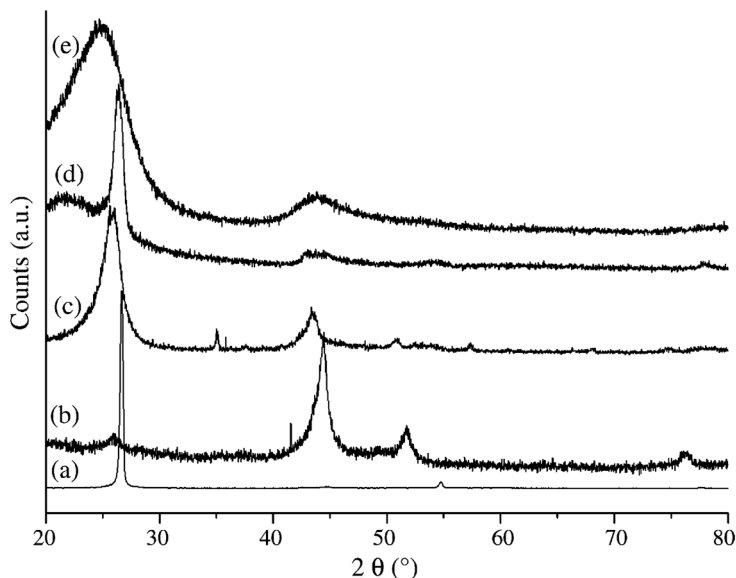


Figure 1.12 X-ray diffraction patterns for (a) graphite; (b) SWNT; (c) MWNT; (d) nanofiber and (e) carbon black. Reproduced with permission from [119]. Copyright © (2006) Elsevier.

accurately from diffraction patterns. It is a fast and non-destructive qualitative tool for routine analysis [120]. Figure 1.12 shows typical XRD patterns for graphite, SWNT, MWNT, carbon nanofiber and carbon black. Pure graphite displays a sharp characteristic peak at 26.6° , corresponding to the (002) diffracting plane. For SWNT, the (002) peak becomes broadened and weakened, and the peak position shifts from 26.6° to $\sim 26^\circ$. This is attributed to the high curvature and high strain energy resulting from small diameters of SWNTs. Other peaks at 44.5° and 51.7° are also observed, corresponding to the $\{(100), (101)\}$, and (004) crystallographic planes. For MWNT, the shape, width and intensity of (002) peak are modified with the increase in the diameter of the nanotube [119]. The (002) peak shifts to $\sim 26.2^\circ$ with respect to that of graphite, and appears slightly asymmetric towards lower angles. The asymmetry is due to the presence of different crystalline species [120, 126].

Ultraviolet-visible-near infrared (UV-vis-NIR) spectroscopy can provide quantitative analysis of the SWNT purity by characterizing their electronic band structures. Because of the one-dimensional structure of SWNTs, the electronic density of state displays several spikes. Accordingly, SWNTs exhibit characteristic electronic transitions associated with Van Hove singularities in the density of states [127]. Semiconducting SWNTs display their first interband transition at S_{11} and second transition at S_{22} , whereas metallic SWNTs show their first transition at M_{11} . Such allowed interband transitions between spikes in the electronic density of states occur in the visible and NIR regions. Figure 1.13 shows a schematic diagram of the absorption

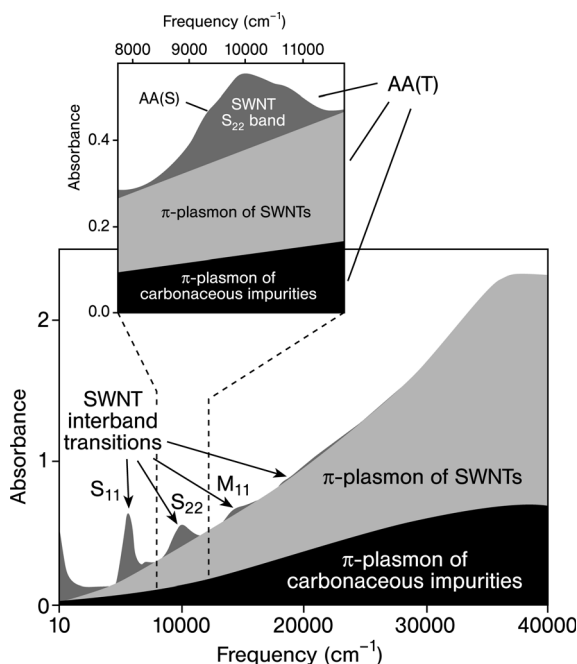


Figure 1.13 Schematic illustration of the electronic spectrum of a typical arc-grown SWNT sample. The inset shows the region of S_{22} interband transition utilized for NIR purity evaluation. In the diagram, $AA(S)$ = area of the S_{22} spectral band after linear baseline correction and $AA(T)$ = total area of the S_{22} band including SWNT and carbonaceous impurity contributions. The NIR relative purity is given by $RP = (AA(S)/AA(T))/0.141$. Reproduced with permission from [131]. Copyright © (2005) The American Chemical Society.

spectrum of an arc-grown SWNT sample in the spectral range between the far-IR and the UV ($10\text{--}45\,000\text{ cm}^{-1}$). From the optical absorption spectra of SWNTs in organic solvents such as *N,N*-dimethylformamide (DMF) or *N,N*-dimethylacetamide (DMA) over a spectral range, several researchers accurately determined the mass fraction of SWNTs in the carbonaceous portion of a given sample [128–131].

TGA can be used to determine the amount of residual metal catalyst quantitatively in CNTs. Moreover, the thermal behavior of the purified CNTs can be obtained from TGA measurements in air. The thermal stability can be expressed in terms of the peak maximum of mass derivative (dM/dT) from the differential thermogravimetry (DTG) curves. It is well recognized that different structural forms of carbon species exhibit different oxidation behavior or affinity towards oxygen. Thus, carbonaceous impurities of CNTs oxidize in air at different temperatures. In general, CNTs are considerably less stable than graphite in an oxidative environment, particularly SWNTs. However, MWNTs with larger diameters and less strained structures are more thermally stable than SWNTs [119]. Table 1.4 summarizes typical DTG temperatures for various carbonaceous species formed in electric arc-grown SWNTs.

Table 1.4 Reported DTG results for various impurities in arc-grown SWNTs.

Investigator	DTG peak temperature (°C)	Carbonaceous and metal species
Hou <i>et al.</i> [111]	385	Oxidation of metal catalyst
	530	Amorphous carbon, carbon nanoparticle
	830	SWNT
Harutyunyan <i>et al.</i> [132]	~350	Amorphous carbon
	~400	SWNT
	~450	Multi-shell carbon
Shi <i>et al.</i> [133]	364	Amorphous carbon
	434	SWNT
Itkis <i>et al.</i> [131]	349	Amorphous carbon
	418	SWNT

The advantages and drawbacks of the analytical techniques mentioned above for the characterization of purified CNTs are well documented in the literature [119, 120, 131]. Recently, NASA-Johnson Space Center has developed a protocol for the characterization of purified and raw HiPco SWNTs [134]. This protocol summarizes and standardizes analytical procedures in TEM, SEM, Raman, TGA and UV-vis-NIR measurements both qualitatively and quantitatively for characterizing the material quality of SWNTs (Table 1.5).

Table 1.5 A protocol developed by NASA-Johnson Space Center for the characterization of purified and raw HiPco SWNTs.

Parameter	Technique	Analysis
Purity	TGA	Quantitative-residual mass after TGA in air at 5 °C min ⁻¹ to 800 °C
	SEM/TEM	Qualitative-amorphous carbon impurities
	EDS	Qualitative-metal content
	Raman	Qualitative-relative amount of carbon impurities and damage/disorder
Thermal stability	TGA	Quantitative-burning temperature in TGA in air at 5 °C min ⁻¹ to 800 °C, dM/dT peak maximum
Homogeneity	TGA	Quantitative-standard deviation of burning temperature and residual mass taken on 3–5 samples
	SEM/TEM	Qualitative-Image comparison
Dispersability	Ultra-sonication	Qualitative-time required to fully disperse (to the eye) low conc. SWCNT in DMF using standard settings
	UV-vis-NIR	Quantitative-relative change in absorption spectra of sonicated low concentration SWCNT/DMF solution

Reproduced with permission from [134]. Copyright © (2004) Elsevier.

1.5

Mechanical Properties of Carbon Nanotubes

1.5.1

Theoretical Modeling

The sp^2 carbon–carbon bond of the basal plane of graphite is considered to be one of the strongest in solid materials. Thus, a rolled-up CNT in which all the basal planes run parallel to the tube axis is expected to yield exceptionally high stiff and strong mechanical properties. It is widely recognized that the elastic modulus of a material is closely related to the chemical bonding of constituent atoms. Mutual interatomic interactions can be described by the relevant force potentials associated with chemical bonding. The elastic modulus of covalently bonded materials depends greatly on the interatomic potential energy derived from bond stretching, bending and torsion. In this case, atomic-scale modeling can be used to characterize the bonding, structure and mechanical properties of CNTs.

Theoretical studies of the elastic behavior of CNTs are mainly concentrated on the adoption of different empirical potentials, and continuum mechanics models using elasticity theory [135–139]. Elastic beam models are adopted because CNTs with very large aspect ratios can be considered as continuum beams. These studies show that CNTs are very flexible, capable of undergoing very large scale of deformation during stretching, twisting or bending. This is in sharp contrast to conventional carbon fibers that fracture easily during mechanical deformation.

Yakobson *et al.* used MD simulation to predict the stiffness, and deformation of SWNTs under axial compression [135]. The carbon–carbon interaction was modeled by Tersoff–Brenner potential, which reflects accurately the binding energies and elastic properties of graphite. The predicted Young's modulus value is rather large, at 5.5 TPa. From the plot of strain energy versus longitudinal strain curve, a series of discontinuities is observed at high strains. An abrupt release in strain energy and a singularity in the strain energy vs strain curve are explained in terms of the occurrence of buckling events. Carbon nanotube has the ability to reversibly buckle by changing its shape during deformation. The simulation also reveals that CNTs can sustain a large strain of 40% with no damage to its graphitic arrangement. Thus, CNTs are extremely resilient, and capable of sustaining extremely large strain without showing signs of brittle fracture. Carbon nanotubes only fracture during axial tensile deformation at very high strains of 30% [136]. Iijima *et al.* used computer simulation to model the bending behavior of SWNTs of varying diameters and helicity [137]. They also adopted the Tersoff–Brenner potential for the carbon–carbon interactions. The prediction also shows that CNTs are extremely flexible when subjected to deformation of large strains. The hexagonal network of nanotubes can be retained by bending up to $\sim 110^\circ$, despite formation of a kink. The kink allows the nanotube to relax elastically during compression. The simulation is further substantiated by HRTEM observation. From these, it can be concluded that SWNT develops kinks in compression and bending, flattens into deflated ribbon under torsion, and still can reversibly restore its original shape.

Hernandez *et al.* used a tight-binding model to predict the Young's modulus of SWNTs. The modulus was found to be dependent on the size and chirality of the nanotubes, ranging from 1.22 TPa for the (10,0) and (6,6) tubes to 1.26 TPa for the (20,0) tube [138]. Lu used the empirical force-constant model to determine the elastic modulus of SWNTs and MWNTs [139]. They reported that the elastic modulus of SWNTs and MWNTs are insensitive to the radius, helicity, and the number of walls. Young's modulus of ~ 1 TPa and shear modulus of ~ 0.5 TPa were determined from such model. Recently, Natsuki *et al.* proposed a continuum-shell approach that links molecular and solid mechanics to predict the Young's modulus and shear modulus of SWNTs [140]. SWNT is regarded as discrete molecular structures linked by carbon-to-carbon bonds. Based on this model, the axial modulus was found to decrease rapidly with increasing nanotube diameter. The shear modulus was about half of the Young's modulus. The axial and shear moduli were predicted in the range of 0.61–0.48 TPa, and 0.30–0.27 TPa, respectively.

1.5.2

Direct Measurement

As mentioned above, Yakobson *et al.* and Iijima *et al.* reported that CNTs are extremely flexible when subjected to deformation of large strains on the basis of MD simulations [135, 137]. Falvo *et al.* used atomic force microscopy (AFM) to investigate the bending responses of MWNTs under large strains [141]. They demonstrated that MWNTs can bend repeatedly through large angles using the tip of an atomic force microscope, without suffering catastrophic failure (Figure 1.14(a)–(d)).

Treacy *et al.* first determined the Young's modulus of arc-grown MWNTs by measuring the amplitude of thermally excited vibrations of nanotubes in a TEM [142]. The nanotubes were assumed equivalent to clamped homogeneous cylindrical cantilevers. TEM images were taken near the tips of free-standing nanotubes. MWNTs were heated from room temperature to 800 °C in steps of 25 °C. Thermal vibrations blurred the image of the tips. The Young's modulus was determined from the slope of the plot of mean-square vibration amplitude (with parameter containing tube length, inner and outer tube diameters) versus temperature. This produced values ranging from 0.4 to 3.70 TPa, with an average value of 1.8 TPa. A large spread in stiffness values arises from the inevitable experimental uncertainties in the estimation of the nanotube length. Another drawback of this method is that the mechanical strength of CNTs cannot be measured. Using the same technique, they obtained a Young's modulus of $1.25\text{--}0.35 / + 0.45$ TPa for SWNTs [143].

According to classical continuum mechanics, the elastic modulus of a beam clamped at one or both ends under a given force can yield vertical deflection. Knowing the deflection of a beam, the elastic modulus can be determined from related mathematical equations. Wong *et al.* employed AFM to determine the elastic modulus and bending strength of arc-grown MWNTs pinned at one end to molybdenum disulfide surface [144]. The nanotubes were then imaged by AFM, allowing the free nanotube to be located. The bending force was measured versus displacement along the unpinned lengths. From the experimental force-displacement curves

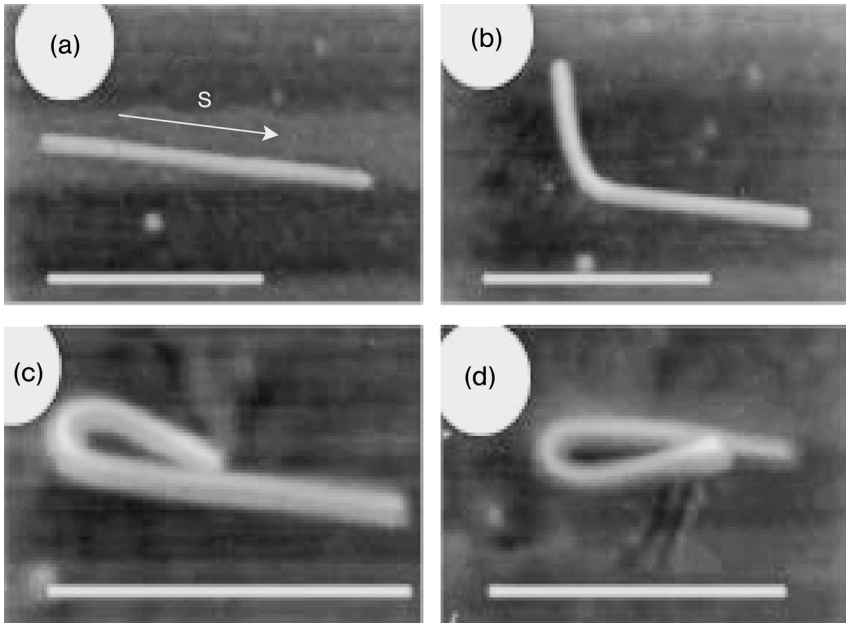


Figure 1.14 Carbon nanotubes in highly strained configuration. The white scale bars at the bottom of each figure represent 500 nm. (a) The original shape of MWNT, 10.5 nm in diameter and 850 nm long. The tube is bent in steps, first upwards (b), until it bends all the way back onto itself (c). The tube is then bent all the way back the other way onto itself (d), to a final curvature similar to that in (c). Reproduced with permission from [141]. Copyright © (1997) Nature Publishing Company.

and mathematical equations based on continuum mechanics, they determined the stiffness to be 1.28 TPa. The bending strength was found to be 14 GPa. Salvetat *et al.* also used AFM to determine the stiffness of the arc- and CVD- grown MWNTs. The nanotube was clamped at both ends during the measurements [145]. A Si_3N_4 microscope tip was employed to apply the force and for measuring the deflection of the CNT. They obtained an average modulus value of 810 GPa for arc-grown MWNT, and 27 GPa for CVD-MWNT. They attributed the lower stiffness of CVD-MWNT to the formation of defect or structural disorder in the tube. On the basis of TEM observation the graphitic planes are tilted with an angle of 30° with respect to the tube axis. Yu *et al.* performed *in situ* tensile measurements in a scanning electron microscope, yielding stiffness values range from 270 to 950 GPa for arc-grown MWNT [146]. They also demonstrated that the MWNT break in the outermost layer, resulting in the morphology commonly described as “sword-in-sheath” feature. The tensile strength of this layer ranges from 11 to 63 GPa.

In general, SWNTs always agglomerate to form ropes with diameters of several tens of nanometers. Using the same equipment, Yu *et al.* obtained an average Young’s modulus of 1 TPa and tensile strength of 30 GPa for SWNT ropes [147]. The tensile strength of SWNT ropes is over 40 times the tensile strength (745 MPa) of typical annealed low alloy steels such as SAE 4340. Low alloys steels are extensively used in

Table 1.6 Experimental Young's modulus and tensile strength of carbon nanotubes synthesized from different techniques.

Investigator	Young's modulus (TPa)	Tensile strength (GPa)	Nanotube type	Synthesis process	Test method
Treacy <i>et al.</i> [142]	1.8	—	MWNT	Electric arc	TEM (thermal vibration)
Krishnam <i>et al.</i> [143]	1.25	—	SWNT	Laser ablation	TEM (thermal vibration)
Wong <i>et al.</i> [144]	1.28	—	MWNT	Electric arc	AFM
Salvetat <i>et al.</i> [145]	0.81	—	MWNT	Electric arc	AFM
Salvetat <i>et al.</i> [145]	0.027	—	MWNT	CVD	AFM
Yu <i>et al.</i> [146]	0.27–0.95	11–63	MWNT	Electric Arc	SEM (tension)
Yu <i>et al.</i> [147]	1	30	SWNT rope	Laser ablation	SEM (tension)
Xie <i>et al.</i> [148]	0.45	3.6	MWNT bundle	CVD	SEM (tension)
Demczyk <i>et al.</i> [149]	0.9	150	MWNT	Electric Arc	TEM (tension)

the manufacture of automotive parts that require high strength and toughness. Xie *et al.* also determined the stiffness of aligned CVD-MWNT bundle employing a technique similar to Yu *et al.* [148]. Recently, Demczyk *et al.* performed *in situ* tension measurement in a TEM for arc-grown MWNT, producing a stiffness of 0.9 TPa and a tensile strength of 0.15 TPa [149]. The results of these investigators are summarized in Table 1.6. From the above discussion, both theoretical and experimental studies confirm that nanotubes have exceptional stiffness and strength. However, a large variation in experimentally measured stiffness and strength is observed, particularly a noticeable reduction in stiffness for CVD-MWNTs when compared with arc-grown MWNTs. This can be expected as these reported values are obtained from a variety of CNTs synthesized from various techniques having different lengths, diameters, disorder structures, level of metal impurities and carbonaceous species.

As mentioned above, the fracture tensile strain of CNTs predicted by the MD simulations could reach up to 30% [136], or even higher depending on simulated temperature and interatomic potential model adopted [150]. Recently, Huang *et al.* reported that the SWNT fractured at room temperature with a strain $\geq 15\%$ [151]. However, the fracture tensile strain of SWNT could reach up to 280% at temperatures $\geq 2000^\circ\text{C}$. (Figure 1.15). In other words, CNT deformed in a superplastic mode at elevated temperatures. In the measurement, a piezo manipulator was used to pull the SWNT to increase the strain under a constant bias of 2.3 V inside a TEM. The temperatures are estimated to be $\geq 2000^\circ\text{C}$ under a bias of 2.3 V. As a result, kinks and point defects are fully activated in the nanotube, resulting in superplastic deformation.

For VGCFs, the modulus has a strong dependence on the graphite plane misorientation [13]. This is because VGCFs are formed by stacking graphite layers into cone and cup structures. The graphite layers are not parallel to the fiber axis. Accordingly, a wide range of stiffness values have been reported in the literature.

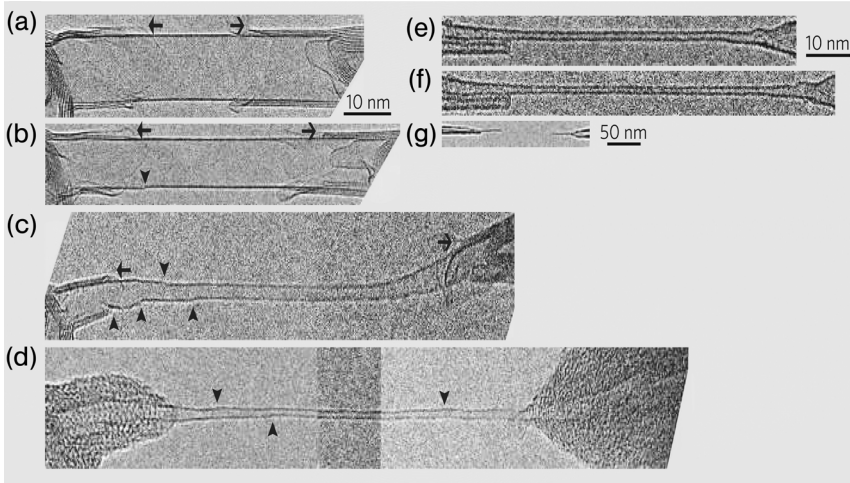


Figure 1.15 *In situ* tensile deformation of individual single-walled CNT in a transmission electron microscope. (a)–(d) Tensile elongation of a SWNT under a constant bias of 2.3 V. Arrowheads mark kinks and arrows indicate features at the ends of the nanotube that are almost unchanged during elongation. Images are scaled to the same magnification.

(e), (f) Tensile elongation of a SWNT at room temperature without bias. Images are scaled to the same magnification. (g) Low magnification image showing fracture in midsection of a nanotube at room temperature. Reproduced with permission from [151]. Copyright © (2006) Nature Publishing Company.

Jacobsen *et al.* used the vibration-reed method to measure the stiffness of VGCF and found an average elastic modulus of 680 GPa [152]. Ishioka *et al.* reported that straight VGCFs have an average Young's modulus of 163 GPa and an average tensile strength of 2.05 GPa based on tensile measurements. Further, impurities and metal catalysts in VGCFs can result in very low stiffness [153]. Uchida *et al.* calculated the elastic modulus of the two-layered nanofiber to be 100–775 GPa, depending on the degree of misorientation of graphite layers [13].

1.6 Physical Properties of Carbon Nanotubes

1.6.1 Thermal Conductivity

The in-plane thermal conductivity of graphite crystal is very high, that is, $\sim 3080\text{--}5150 \text{ W m}^{-1}\text{K}^{-1}$ at room temperature [154]. However, the c-axis thermal conductivity of graphite is very low because its interlayer is bounded by weak van der Waals forces [155]. The thermal conductivity of graphite generally increases markedly as the temperature is reduced [156], and closely related to their lattice vibrations or phonons. Contribution to a finite in-plane thermal conductivity of graphite at low

temperatures is considered to be associated with acoustic phonon scattering. The thermal conductivity of two-dimensional graphite sheet exhibits quadratic temperature dependence at low temperatures. At higher temperatures (say above 140 K), phonon–phonon (umklapp) scattering process dominates.

Berber *et al.* demonstrated that CNTs have an unusually high thermal conductivity on the basis of MD simulation. The predicted conductivity of SWNT is $6600 \text{ W m}^{-1}\text{K}^{-1}$ at room temperature [157]. This value is much higher than that of graphite and diamond. The high thermal conductivity of SWNT is believed to result from the large phonon mean free path in one-dimensional nanostructure. The theoretical phonon mean free path length of SWNTs could reach a few micrometers [158]. Considering the umklapp phonon scattering process, Cao *et al.* developed a model to analyze the thermal transport in a perfect isolated SWNT [159]. They reported that the thermal conductivity of an isolated SWNT increases with the increase of temperature at low temperatures, and shows a peaking behavior at about 85 K before falling off at higher temperatures. The thermal transport in the SWNT is dominated by phonon boundary scattering at low temperatures. As temperature increases, umklapp scattering process becomes stronger and contributes to the heat transfer. Further, SWNTs with small diameters exhibit higher thermal conductivity that is inversely proportional to the tube's diameter at 300 K.

Yie *et al.* determined the thermal conductivity MWNT bundles using a self-heating 3ω method [160]. The thermal conductivity is approximately linear at temperatures above 120 K, but becomes quadratic at temperatures below that. Subsequently, Kim *et al.* measured the thermal conductivity of an individual MWNT using a microfabricated suspended device. The observed thermal conductivity is higher than $3000 \text{ W m}^{-1}\text{K}^{-1}$ at room temperature and the phonon mean free path is $\sim 500 \text{ nm}$ [161]. The conductivity value is two orders of magnitude higher than the estimation from previous researchers using macroscopic mat samples ($\sim 35 \text{ W m}^{-1}\text{K}^{-1}$ for SWNTs [162]). Moreover, the measurements shows a nearly T^2 -dependence of thermal conductivity for $50 \text{ K} < T < 150 \text{ K}$. Above 150 K, thermal conductivity deviates from quadratic temperature dependence and displays a peak at 320 K due to the onset of umklapp phonon–phonon scattering. It is noted that the clustering of MWNTs into bundles tends to reduce their thermal conductivity, but has no effect on the temperature dependence of conductivity [148, 158]. When the MWNTs are consolidated into bulk specimens by spark plasma sintering (SPS), the thermal conductivity becomes even lower as a result of the tube–tube interactions [163, 164]. Table 1.7 summarizes the reported thermal conductivity of CNTs synthesized from different processes. Apparently, the thermal conductivity of individual carbon nanotube ($3000 \text{ W m}^{-1}\text{K}^{-1}$) is significantly higher than silver and copper metals having the highest conductivity of about $400 \text{ W m}^{-1}\text{K}^{-1}$.

1.6.2

Electrical Behavior

Because of the anisotropic nature of graphite, the in-plane electrical conductivity of graphite crystal is very high as a result of the overlap of π orbitals of the adjacent

Table 1.7 Theoretical and experimental thermal conductivity at room temperature for carbon nanotubes fabricated from different techniques.

Material	Fabrication process	Measurement technique	Thermal conductivity ($\text{W m}^{-1} \text{K}^{-1}$)
Individual SWNT [157]	—	MD simulation	6600
Individual MWNT [161]	—	Microfabricated device	3000
MWNT bundle [160]	CVD	Self-heating 3ω method	25
SWNT mat [162]	Arc-discharge	Comparative method	35
Bulk MWNT [163]	SPS (2000 °C, 50 MPa, 3 min)	Laser-flash	4.2
Bulk MWNT [164]	SPS (1700 °C, 50 MPa)	Laser-flash	2.15

carbon atoms. However, the mobility perpendicular to the planes is relatively low [165].

As mentioned before, the electrical properties of CNTs vary from metallic to semiconducting, depending on the chirality and diameter of CNTs. Both theoretical and experimental measurement results demonstrate the superior electrical properties of CNTs. MWNTs can carry extremely high current density from 10^7 to 10^9 A cm^{-2} [166, 167]. The reported room temperature resistivity of individual carbon nanotube is in the order of 10^{-6} – $10^{-4} \Omega \text{ cm}$ [168]. Smalley's group measured the resistivity of metallic SWNT ropes using a four-point technique. The resistivity was found to be $\sim 10^{-4} \Omega \text{ cm}$ at 300 K [169, 170]. These properties make CNTs the most conductive tubes/wires ever known.

The electrons in one-dimensional CNTs are considered to be ballistically conducted. This implies that the electrons with a large phase coherence length experience no scattering from phonons during ballistic transport in CNTs. Therefore, electrons encounter no resistance and dissipate no heat in CNTs. In this respect, the conductance (the inverse of resistance) of individual SWNTs is predicted to be quantized with a value of $2G_0$, independent of the diameter and the length [171]. The conductance quantum (G_0) can be expressed by the following equation:

$$G_0 = 2e^2/h = (12.9 \text{ k}\Omega)^{-1} \quad (1.7)$$

where e is the electronic charge and h is Planck's constant.

Frank *et al.* measured the conductance of MWNTs using a scanning probe microscope attached with a nanotube fiber. The fiber was carefully dipped into the liquid mercury surface [166]. After contact was established, the current was measured as a function of the position of the nanotubes in the mercury. The results revealed that the nanotubes conduct current ballistically with quantized conductance behavior. The MWNT conductance jumped by increments of one unit of G_0 . Recently, Urbina *et al.* also observed quantum conductance steps of MWNTs in a mixture of polychlorinated biphenyls [172].

Carbon nanotubes with high aspect ratio exhibit excellent field emission characteristics. Electrons can be emitted readily from the nanotube tips by applying a potential between the nanotube surface and an anode. CNTs have been considered as field electron emission Sources for field emission displays (FED), backlights for liquid crystal displays, outdoor displays and traffic signals [173]. However, few FED devices based on CNTs are available commercially because it is difficult to control the properties of CNTs and there is fierce competition with existing organic light-emitting diodes and plasma display panels [174].

1.7

Potential and Current Challenges

A brief overview of the latest state-of-the-art advances in the synthesis, purification, materials characterization, mechanical and physical behavior of CNTs has been presented. It is evident that there is a wealth of synthetic strategies in the development of CNTs but attention is currently focused on both the improvement and simplicity of existing synthetic techniques. Advances in the synthesis of CNTs have continued to improve rapidly in recent years. There are still many challenges to be resolved in their synthesis, purification and cost-effective production processes. Some research efforts are currently underway to overcome these challenges. The price of CNTs, especially SWNTs, is still very expensive when compared with other inorganic fillers commonly used to reinforce metals or ceramics. The price of SWNT is US\$ 9990 per 100 g [175]. This has so far restricted their prospects as a substitution for inorganic fillers in composite industries. Furthermore, CNTs synthesized from various techniques contain different levels of metal impurities, amorphous carbon and other carbonaceous byproducts. Purification and subsequent materials examination of nanotubes are costly and time consuming. It is necessary to bring the cost of nanotubes down to an acceptable level through novel innovation of large-scale fabrication and simplified purification processes to manufacture nanotubes of high quality and purity.

Developing high-performance nanocomposites for advanced engineering applications requires the ability to tailor their microstructure, mechanical and physical properties. The successful implementation of such nanocomposites depends on the development of novel processing techniques and fundamental understanding of their structure–property relationship. The development and synthesis of metal- and ceramic nanocomposites is still in the embryonic stage. One of the most important challenges in the fabrication of nanocomposites is how to achieve homogeneous dispersion of nanotubes within a metallic or ceramic matrix. Owing to their tangled feature and large surface area, CNTs tend to disperse as agglomerates or clusters in metals or ceramics during processing. Agglomeration of nanotubes can lead to resulting composites having inferior mechanical strength and toughness as well as poor physical properties. Uniform distribution of nanotubes in metal or ceramic matrix is essential to achieve effective load-bearing capacity of the reinforcement. Therefore, microstructural control is crucial to obtain optimal mechanical and physical properties in metal- and ceramic nanocomposites.

Nomenclature

\vec{a}_1, \vec{a}_2	Unit vectors in two-dimensional hexagonal lattice
\vec{C}_h	Chiral vector
d	Diameter of carbon nanotube
e	Electronic charge
G_o	Conductance quantum (G_o)
h	Planck's constant.
n, m	Integers
θ	Chiral angle

References

- 1 Tjong, S.C. (2007) Novel nanoparticle-reinforced metal matrix composites with enhanced mechanical properties. *Advanced Engineering Materials*, **9**, 588–593.
- 2 Ma, Z.Y., Li, Y.L., Liang, Y., Zheng, F., Bi, J. and Tjong, S.C. (1996) Nanometric Si_3N_4 particulate-reinforced aluminum composite. *Materials Science and Engineering A*, **219**, 229–231.
- 3 Ma, Z.Y., Tjong, S.C. and Li, Y.L. (1999) The performance of aluminum-matrix composites with nanometric particulate Si-N-C reinforcement. *Composites Science and Technology*, **59**, 263–270.
- 4 Kang, Y.C. and Chan, S.L. (2004) Tensile properties of nanometric Al_2O_3 particulate-reinforced aluminum matrix composites. *Materials Chemistry and Physics*, **85**, 438–443.
- 5 Ijima, F. S. (1991) Helical microtubules of graphite carbon. *Nature*, **354**, 56–68.
- 6 Tjong, S.C. (2006) Structural and mechanical properties of polymer nanocomposites. *Materials Science and Engineering R*, **53**, 73–197.
- 7 Tjong, S.C., Liang, G.D. and Bao, S.P. (2007) Electrical behavior of polypropylene/multi-walled carbon nanotube nanocomposites with low percolation threshold. *Scripta Materialia*, **57**, 461–464.
- 8 Tjong, S.C., Liang, G.D. and Bao, S.P. (2008) Effects of crystallization on dispersion of carbon nanofibers and electrical properties of polymer nanocomposites. *Polymer Engineering and Science*, **48**, 177–183.
- 9 Heimann, R.B., Evsyukov, S.E. and Koga, Y. (1997) Carbon allotropes: A suggested classification scheme based on valence orbital hybridization. *Carbon*, **35**, 1654–1658.
- 10 Kroto, H.W., Heath, J.R., O'Brien, S.C., Curl, R.F. and Smalley, R.H. (1985) C-60-buckminsterfullerene. *Nature*, **318**, 162–163.
- 11 Rao, C.N., Seshadri, R., Govindaraj, A. and Sen, R. (1995) Fullerenes, nanotubes, onions and related carbon structures. *Materials Science and Engineering R*, **15**, 209–262.
- 12 Yamabe, T. (1995) Recent development of carbon nanotubes. *Synthetic Metals*, **70**, 1511–1518.
- 13 Uchida, T., Anderson, D.P., Minus, M.L. and Kumar, S. (2006) Morphology and modulus of vapor grown carbon nanofibers. *Journal of Materials Science*, **41**, 5851–5856.
- 14 Melechko, A.V., Merkulov, V.I., McKnight, T.E., Guillorn, M.A., Klein, K.L., Lowndes, D.H. and Simpson, M.L. (2005) Vertically aligned carbon nanofibers and related structures:

- Controlled synthesis and directed assembly. *Journal of Applied Physics*, **97**, 041301(1)–041301(39).
- 15 Thostenson, E., Ren, Z. and Chou, T. (2001) Advances in science and technology of carbon nanotubes and their applications: a review. *Composites Science and Technology*, **61**, 1899–1912.
 - 16 Dresselhaus, M.S., Dresselhaus, G. and Saito, R. (1995) Physics of carbon nanotubes. *Carbon*, **33**, 883–891.
 - 17 Tibbets, G.G. (1989) Vapor-grown fibers: status and prospects. *Carbon*, **27**, 745–747.
 - 18 Laplaze, D., Bernier, P., Maser, W.K., Flamant, G., Guillard, T. and Loiseau, A. (1998) Carbon nanotubes: The solar approach. *Carbon*, **36**, 685–688.
 - 19 Ebbesen, T.W. (1994) Carbon nanotubes. *Annual Review of Materials Science*, **24**, 235.
 - 20 Iijima, S., Ajayan, P.M. and Ichihashi, T. (1992) Growth model for carbon nanotubes. *Physical Review Letters*, **69**, 3100–3103.
 - 21 Iijima, S. (1993) Growth of carbon nanotubes. *Materials Science and Engineering B*, **19**, 172–180.
 - 22 Ebbesen, T.W. and Ajayan, P.M. (1992) Large-scale synthesis of carbon nanotubes. *Nature*, **358**, 220.
 - 23 Lee, S.J., Baik, H.K., Yoo, J.E. and Han, J.H. (2002) Large scale synthesis of carbon nanotubes by plasma rotating arc discharge technique. *Diamond and Related Materials*, **11**, 914–917.
 - 24 Jung, S.H., Kim, M.R., Jeong, S.H., Kim, S.U., Lee, O.J., Lee, K.H., Suh, J.H. and Park, C.K. (2003) High-yield synthesis of multi-walled carbon nanotubes by arc discharge in liquid nitrogen. *Applied Physics A*, **76**, 285–286.
 - 25 Iijima, S. and Ichihashi, T. (1993) Single-shell carbon nanotubes of 1-nm diameter. *Nature*, **363**, 603–605.
 - 26 Bethune, D.S., Kiang, C.H., de Vries, M.S., Gorman, G., Savoy, R., Vasquez, J. and Beyers, R. (1993) Cobalt-catalyzed growth of carbon nanotubes with single-atomic-layer walls. *Nature*, **363**, 603–605.
 - 27 Ajayan, P.M., Lambert, J.M., Bernier, P., Barbedette, L., Colliex, C. and Planeix, J.M. (1993) Growth morphologies during cobalt-catalyzed single-shell carbon nanotube synthesis. *Chemical Physics Letters*, **215**, 509–517.
 - 28 Journet, C. and Bernier, P. (1998) Production of carbon nanotubes. *Applied Physics A*, **67**, 1–9.
 - 29 Saito, Y., Nishikubo, K., Kawabata, K. and Matsumoto, T. (1996) Carbon nanocapsules and single-layered nanotubes produced with platinum-group metals (Ru, Rh, Pd, Os, Ir, Pt) by arc discharge method. *Journal of Applied Physics*, **80**, 3062–3067.
 - 30 Zhao, X., Ohkohchi, M., Inoue, S., Suzuki, T., Kadoya, T. and Ando, Y. (2006) Large-scale purification of single-wall nanotubes prepared electric arc discharge. *Diamond and Related Materials*, **15**, 1098–1102.
 - 31 Farhat, S., de La Chapelle, M.L., Loiseau, A., Scott, C.D., Lefrant, S., Journet, C. and Bernier, P. (2001) Diameter control of single-walled carbon nanotubes using argon-helium mixtures gases. *Journal of Chemical Physics*, **115**, 6752–6759.
 - 32 Lambert, J.M., Ajayan, P.M., Bernier, P., Planeix, J.M., Brontons, V., Coq, B. and Castaing, J. (1994) Improving conditions towards isolating single-shell carbon nanotubes. *Chemical Physics Letters*, **226**, 364–371.
 - 33 Guo, T., Nikolev, P., Thess, A., Colbert, D.T. and Smalley, R.E. (1995) Catalytic growth of single-walled nanotubes by laser vaporization. *Chemical Physics Letters*, **243**, 49–54.
 - 34 Scott, C.D., Arepalli, S., Nikolaev, P. and Smalley, R.E. (2001) Growth mechanisms for single-wall carbon nanotubes in a laser-ablation process. *Applied Physics A*, **72**, 573–580.
 - 35 Bandow, S. and Asaka, S. (1998) Effect of growth temperature on the diameter distribution and chirality of single-wall

- carbon nanotubes. *Physical Review Letters*, **80**, 3779–3782.
- 36 Yudasaka, M., Yamada, R., Sensui, N., Wilkins, T., Ichihashi, T. and Iijima, S. (1999) Mechanism of the effect of NiCo, Ni and Co catalysts on the yield of single-wall carbon nanotubes formed by pulsed Nd:YAG laser ablation. *The Journal of Physical Chemistry B*, **103**, 6224–6229.
- 37 Dillon, A.C., Parilla, P.A., Alleman, J.L., Perkins, J.D. and Heben, M.J. (2000) Controlling single-wall nanotube diameters with variation in laser pulse power. *Chemical Physics Letters*, **316**, 13–18.
- 38 Braidy, N., El Khakani, M.A. and Botton, G.A. (2002) Single-wall carbon nanotubes synthesis by means of UV laser vaporization. *Chemical Physics Letters*, **354**, 88–92.
- 39 Kusaba, M. and Tsunawaki, Y. (2006) Production of single-wall carbon nanotubes by a XeCl excimer laser ablation. *Thin Solid Films*, **506–507**, 255–258.
- 40 Kusaba, M. and Tsunawaki, Y. (2007) Raman spectroscopy of SWNTs produced by a XeCl excimer laser ablation at high temperatures. *Applied Surface Science*, **253**, 6330–6333.
- 41 Maser, W.K., Munoz, E., Benito, A.M., Martinez, M.T., de la Fuente, G.F., Maniette, Y., Anglaret, E. and Sauvajol, J.L. (1998) Production of high-density single-walled nanotube material by a simple laser-ablation method. *Chemical Physics Letters*, **292**, 587–593.
- 42 Bolshakov, A.P., Uglov, S.A., Saveliev, A.V., Konov, V.I., Gorbunov, A.A., Pompe, W. and Graff, A. (2002) A novel CW laser-powder method of carbon single-wall nanotube production. *Diamond and Related Materials*, **11**, 927–930.
- 43 Dillon, A.C., Parilla, P.A., Jones, K.M., Riker, G. and Heben, M.J. (1998) A comparison of single-wall carbon nanotube production using continuous and pulsed laser vaporization. *Materials Research Society Symposium Proceedings*, **526**, 403–408.
- 44 Elkund, P.C., Pradhan, B.K., Kim, U.J., Xiong, Q., Fischer, J.E., Friedman, A.D., Holloway, B.C., Jordan, K. and Smith, M.W. (2002) Large-scale production of single-walled carbon nanotubes using ultrafast pulses from a free electron laser. *Nano Letters*, **2**, 561–566.
- 45 Kukovitsky, E.F., L'vov, S.G. and Sainov, N.A. (2000) VLS-growth of carbon nanotubes from the vapor. *Chemical Physics Letters*, **317**, 65–70.
- 46 Gruneis, A., Kramberger, C., Grimm, D., Gemming, T., Rummeli, M.H., Barreiro, A., Ayala, P., Pichler, T., Schaman, C., Kuzmany, H., Schumann, J. and Buchner, B. (2006) Eutectic limit for the growth of carbon nanotubes from a thin iron film by chemical vapor deposition of cyclohexane. *Chemical Physics Letters*, **425**, 301–305.
- 47 Kwok, K. and Chiu, W.K. (2005) Growth of carbon nanotubes by open-air laser-induced chemical vapor deposition. *Carbon*, **43**, 437–446.
- 48 Wagner, R.S. and Ellis, W.C. (1964) Vapor-liquid-solid mechanism of single crystal growth. *Applied Physics Letters*, **4**, 89–90.
- 49 Wu, Y. and Yang, P. (2001) Direct observation of vapor-liquid-solid nanowire growth. *Journal of the American Chemical Society*, **123**, 3165–3166.
- 50 Ohring, F.M. (ed) (2002) *Materials Science of Thin Film: Deposition and Structure*, Academic Press, San Diego, USA.
- 51 Zaretskiy, S.N., Hong, Y.K., Dong, H.H., Yoon, J.H., Cheon, J. and Koo, J.Y. (2003) Growth of carbon nanotubes from Co nanoparticles and C₂H₂ by thermal chemical vapor deposition. *Chemical Physics Letters*, **372**, 300–305.
- 52 Hong, Y.K., Kim, H., Lee, G., Kim, W., Park, J.I., Cheon, J. and Koo, J.K. (2002) Controlled two-dimensional distribution of nanoparticles by spin-coating method. *Applied Physics Letters*, **80**, 844–846.
- 53 Lee, C.J., Lyu, S.C., Cho, Y.R., Lee, J.H. and Cho, K.I. (2001) Diameter-controlled growth of carbon nanotubes using thermal chemical vapor deposition. *Chemical Physics Letters*, **341**, 245–249.

- 54 Choi, Y.C., Shin, Y.M., Lee, Y.H., Lee, B.S., Park, G.S., Choi, W.B., Lee, N.S. and Kim, J.M. (2000) Controlling the diameter, growth rate, and density of vertically aligned carbon nanotubes synthesized by microwave plasma enhanced chemical vapor deposition. *Applied Physics Letters*, **76**, 2367–2369.
- 55 Hernadi, K., Fonseca, A., Nagy, J.B., Bernaerts, D., Fudala, A. and Lucas, A.A. (1996) Catalytic synthesis of carbon nanotubes using zeolite support. *Zeolites*, **17**, 416–423.
- 56 Choi, G.S., Cho, Y.S., Hong, S.Y., Park, J.B., Son, K.H. and Kim, D.J. (2002) Carbon nanotubes synthesized by Ni-assisted atmospheric pressure thermal chemical vapor deposition. *Journal of Applied Physics*, **91**, 3847–3854.
- 57 Sohn, J.I., Choi, C.J., Lee, S. and Seong, T.Y. (2002) Effects of Fe film thickness and pretreatments on the growth behaviors of carbon nanotubes on Fe-doped (001) Si substrates. *Japanese Journal of Applied Physics*, **41**, 4731–4736.
- 58 Ducati, C., Alexandrou, I., Chhowalla, M., Amaratunga, G.A. and Robertson, J. (2002) Temperature selective growth of carbon nanotubes by chemical vapor deposition. *Journal of Applied Physics*, **92**, 3299–3303.
- 59 Li, H., Zhao, N., He, C., Shi, C., Du, X., Li, J. and Cui, Q. (2008) Fabrication of short and straight carbon nanotubes by chemical vapor deposition. *Materials Science and Engineering A*, **476**, 230–233.
- 60 Li, H., Shi, C., Du, X., He, C., Li, J. and Zhao, N. (2008) The influences of synthesis temperature and Ni catalyst on the growth of carbon nanotubes by chemical vapor deposition. *Materials Letters*, **62**, 1472–1475.
- 61 Lee, C.J., Kim, D.W., Lee, T.J., Choi, Y.C., Park, Y.S., Lee, Y.H., Choi, W.B., Lee, N.S., Park, G.S. and Kim, J.M. (1999) Synthesis of aligned carbon nanotubes using thermal chemical vapor deposition. *Chemical Physics Letters*, **312**, 461–468.
- 62 Choi, K.S., Cho, Y.S., Hong, S.Y., Park, J.B. and Kim, D.J. (2001) Effects of ammonia on the alignment of carbon nanotubes in metal-assisted thermal chemical vapor deposition. *Journal of the European Ceramic Society*, **21**, 2095–2098.
- 63 Kayastha, V., Yap, Y.K., Dimovski, S. and Gogotsi, Y. (2004) Controlling dissociative adsorption for effective growth of carbon nanotubes. *Applied Physics Letters*, **85**, 3265–3267.
- 64 Hofmann, S., Ducati, C., Robertson, J. and Kleinsorge, B. (2003) Low-temperature growth of carbon nanotubes by plasma-enhanced chemical vapor deposition. *Applied Physics Letters*, **83**, 135–137.
- 65 Minea, T.M., point, S., Granier, A. and Touzeau, M. (2004) Room temperature synthesis of carbon nanofibers containing nitrogen by plasma-enhanced chemical vapor deposition. *Applied Physics Letters*, **85**, 1244–1246.
- 66 Ikuno, T., Honda, S.I., Kamada, K., Qura, K. and Katayama, M. (2005) Effect of oxygen addition to methane on growth of vertically oriented carbon nanotubes by radio-frequency plasma-enhanced chemical vapor deposition. *Journal of Applied Physics*, **97**, 104329 1–104329 4.
- 67 Eres, G., Puzos, A.A., Geoghegan, D.B. and Cui, H. (2004) *In situ* control of the catalyst efficiency in chemical vapor deposition of vertically aligned carbon nanotubes on predeposited metal catalyst film. *Applied Physics Letters*, **84**, 1759–1761.
- 68 Bell, M.S., Lacerda, R.G., Teo, K.B., Rupasinghe, N.L., Amaratunga, G.A., Molne, W.I. and Chhowalla, M. (2004) Plasma composition during plasma-enhanced chemical vapor deposition of carbon nanotubes. *Applied Physics Letters*, **85**, 1137–1139.
- 69 Hsu, C.M., Lin, C.H., Lai, H.J. and Kuo, C.T. (2005) Root growth of multi-wall carbon nanotubes by MPCVD. *Thin Solid Films*, **471**, 140–144.

- 70 Jang, I., Uh, H.S., Cho, H.J., Lee, W., Hong, J.P. and Lee, N. (2007) Characteristics of carbon nanotubes grown by mesh-inserted plasma-enhanced chemical vapor deposition. *Carbon*, **45**, 3015–3021.
- 71 Wang, X., Hu, Z., Wu, Q., Chen, X. and Chen, Y. (2001) Synthesis of multi-walled carbon nanotubes by microwave plasma-enhanced chemical vapor deposition. *Thin Solid Films*, **390**, 130–113.
- 72 Duty, C., Jean, D. and Lackey, W.J. (2001) Laser chemical vapor deposition: materials, modeling, and process control. *International Materials Reviews*, **46**, 271–287.
- 73 Rohmund, F., Morjan, R., Ledoux, G., Huisken, F. and Alexandrescu, R. (2002) Carbon nanotube films grown by laser-assisted chemical vapor deposition. *Journal of Vacuum Science & Technology B*, **20**, 802–811.
- 74 Bondi, S.N., Lackey, W.J., Johnson, R.W., Wang, X. and Wang, Z.L. (2006) Laser assisted chemical vapor deposition synthesis of carbon nanotubes and their characterization. *Carbon*, **44**, 1393–1403.
- 75 Tibbets, G.G. (1983) Carbon fibers produced by pyrolysis of natural gas in stainless steel tubes. *Applied Physics Letters*, **42**, 666–668.
- 76 Allouche, H., Monthieux, M. and Jacobsen, R.L. (2003) Chemical vapor deposition of pyrolytic carbon on carbon nanotubes. Part 1: Synthesis and morphology. *Carbon*, **41**, 2897–2912.
- 77 <http://www.apsci.com>.
- 78 Tibbets, G.G., Finegan, J.C., McHugh, J.J., Ting, J.M., Glasgow, D.D. and Lake, M.L. (2000) Applications research on vapor-grown carbon fibers, in *Science and Application of Nanotubes* (eds D. S Tomanek and R.J. S Enbody), Kluwer, New York, USA.
- 79 <http://www.electrovac.com>.
- 80 Hammel, E., Tang, X., Trampert, M., Schmitt, T., Mauthner, K., Eder, A. and Potschke, P. (2004) Carbon nanofibers for composite applications. *Carbon*, **42**, 1153–1158.
- 81 Satishkumar, B.C., Govindaraj, A. and Rao, C.N. (1999) Bundles of aligned carbon nanotubes obtained by the pyrolysis of ferrocene-hydrocarbon mixtures: role of the metal nanoparticles produced *in situ*. *Chemical Physics Letters*, **307**, 158–162.
- 82 Jang, J.W., Lee, K.W., Oh, I.H., Lee, E.M., Kim, I.M., Lee, C.E. and Lee, C.J. (2008) Magnetic Fe catalyst particles in vapor phase grown multiwalled carbon nanotubes. *Solid State Communications*, **145**, 561–564.
- 83 Rohmund, F., Falk, L.K. and Campbell, E.E. (2000) A simple method for the production of large arrays of aligned carbon nanotubes. *Chemical Physics Letters*, **328**, 369–373.
- 84 Andrews, R., Jacques, D., Rao, A.M., Derbyshire, F., Qian, D., Fan, X., Dickey, E.C. and Chen, J. (1999) Continuous production of aligned carbon nanotubes: a step closer to commercial production. *Chemical Physics Letters*, **303**, 467–474.
- 85 Wang, Y., Wei, F., Luo, G., Yu, H. and Gu, G. (2002) The large-scale production of carbon nanotubes in a nano-agglomerate fluidized-bed reactor. *Chemical Physics Letters*, **364**, 568–572.
- 86 Nikolaev, P., Bronikowski, M.J., Bradley, R.K., Rohmund, F., Colbert, D.T., Smith, K.A. and Smalley, R.E. (1999) Gas-phase catalytic growth of single-walled nanotubes from carbon monoxide. *Chemical Physics Letters*, **313**, 91–97.
- 87 Dai, H., Rinzler, A.G., Nikolaev, P., Thess, A., Colbert, D.T. and Smalley, R.E. (1996) Single-walled nanotubes produced by metal-catalyzed disproportionation of carbon dioxide. *Chemical Physics Letters*, **260**, 471–475.
- 88 Kitiyanan, B., Alvarez, W.E., Harwell, J.H. and Resasco, D.E. (2000) Controlled production of single-wall carbon nanotubes by catalytic decomposition of CO on bimetallic Co-Mo catalysts. *Chemical Physics Letters*, **317**, 497–503.

- 89 Herrera, J.E., Balzano, L., Borgna, A., Alvarez, W.E. and Resasco, D.E. (2001) Relationship between the structure/ composition of Co-Mo catalysts and their ability to produce single-walled carbon nanotubes by CO disproportionation. *Journal of Catalysis*, **204**, 129–145.
- 90 Resasco, D.E., Alvarez, W.E., Pompeo, F., Balzano, L., Herrera, J.E., Kitiyanan, B. and Borgna, A. (2002) A scalable process for production of single-walled carbon nanotubes (SWNTs) by catalytic disproportionation of CO on a solid catalyst. *Journal of Nanoparticle Research*, **4**, 131–136.
- 91 Kim, Y.N. (2008) Preparation of carbon nanotubes. US Patent 7329398.
- 92 Benavides, J.M. (2006) Method for manufacturing high quality carbon nanotubes. US Patent 7008605.
- 93 Beguin, F., Delpoux, S. and Szostak, K. (2006) Process for the mass production of multiwalled carbon nanotubes. US Patent 7094385.
- 94 Smalley, R.E., Colbert, D.T., Dai, H., Liu, J., Rinzler, A.G., Hafner, J.H., Smith, K., Guo, T., Nikolaev, P. and Thess, A. (2006) Method for forming an array of single-wall carbon nanotubes in an electric field and compositions thereof. US Patent 7087207.
- 95 Resasco, D.E., Kitiyanan, B., Harwell, J.H. and Alvarez, W.E. (2005) Metallic catalytic particle for producing single-walled carbon nanotubes. US Patent 6962892.
- 96 Resasco, D.E., Kitiyanan, B., Harwell, J.H. and Alvarez, W.E. (2006) Carbon nanotubes product comprising single-walled carbon nanotubes. US Patent 6994907.
- 97 Ebbesen, T.W., Ajayan, P.M., Hiura, H. and Tanigaki, K. (1994) Purification of nanotubes. *Nature*, **367**, 319–319.
- 98 Zimmerman, J.L., Bradley, R.K., Huffman, C.B., Hauge, R.H. and Margrave, J.L. (2000) Gas-phase purification of single-walled nanotubes. *Chemistry of Materials*, **12**, 1361–1366.
- 99 Park, Y.S., Choi, Y.C. and Kim, K.S. (2001) High yield purification of multi-walled carbon nanotubes by selective oxidation during thermal annealing. *Carbon*, **39**, 655–661.
- 100 Hiura, H., Ebbesen, T.W. and Tanigaki, K. (1995) Opening and purification of carbon nanotubes in high yields. *Advanced Materials*, **7**, 275–276.
- 101 Rinzler, A., Liu, J., Dai, H., Nikolaev, P., Huffman, C.B., Rodriguez-Macias, F.J., Boul, P.J., Heymann, D., Colbert, D.T., Lee, R.S., Fischer, E., Rao, A.M., Eklund, P.C. and Smalley, R.E. (1998) Large-scale purification of single-walled carbon nanotubes: process, product and characterization. *Applied Physics A*, **67**, 29–37.
- 102 Chiang, I.W., Brinson, B.E. and Smalley, R.E. (2001) Purification and characterization of single-walled carbon nanotubes. *The Journal of Physical Chemistry. B*, **105**, 1157–1161.
- 103 Hernadi, K., Siska, A., Thien-Nga, L., Forro, L. and Kiricsi, I. (2001) Reactivity of different kinds of carbon during oxidative purification of catalytically prepared carbon nanotubes. *Solid State Ionics*, **141–142**, 203–209.
- 104 Chen, C.M., Chen, M., Peng, Y.W., Lin, C.H., Chang, L.W. and Chen, C.F. (2005) Microwave digestion and acidic treatment procedures for the purification of multi-walled carbon nanotubes. *Diamond and Related Materials*, **14**, 798–803.
- 105 Chen, C.M., Chen, M., Peng, Y.W., Yu, H.W. and Chen, C.F. (2006) High efficiency microwave digestion purification of multiwalled carbon nanotubes synthesized by thermal chemical vapor deposition. *Thin Solid Films*, **498**, 202–205.
- 106 Porro, S., Musso, S., Vinante, M., Vanzetti, L., Anderle, M., Trotta, F. and Tagliaferro, A. (2007) Purification of carbon nanotubes grown by thermal CVD. *Physica E*, **37**, 58–61.
- 107 Bandow, S., Rao, A.M., Williams, K.A., Thess, A., Smalley, R.E. and Eklund, P.C. (1999) Purification of single-wall carbon nanotubes by microfiltration. *The Journal of Physical Chemistry. B*, **101**, 8839–8842.

- 108** Shelimov, K.B., Esenaliev, R.O., Rinzler, A.G., Huffman, C.B. and Smalley, R.E. (1998) Purification of single-walled carbon nanotubes by ultrasonically assisted filtration. *Chemical Physics Letters*, **282**, 429–434.
- 109** Li, F., Cheng, H.M., Xing, Y.T., Tan, P.H. and Su, G. (2000) Purification of single-walled carbon nanotubes synthesized by the catalytic decomposition of hydrocarbons. *Carbon*, **38**, 2041–2045.
- 110** Yu, A., Bekyarova, E., Itkis, M.E., Fakhruddinov, D., Webster, R. and Haddon, R.C. (2006) Application of centrifugation to the large-scale purification of electric arc-produced single-walled carbon nanotubes. *Journal of the American Chemical Society*, **128**, 9902–9908.
- 111** Hou, P., Liu, C., Tong, Y., Liu, M. and Cheng, H. (2001) Purification of single-walled nanotubes synthesized by the hydrogen arc-discharge method. *Journal of Materials Research*, **16**, 2526–2529.
- 112** Strong, K.L., Anderson, D.P., Lafdi, K. and Kuhn, J.N. (2003) Purification process for single-walled nanotubes. *Carbon*, **41**, 1477–1488.
- 113** Montoro, L.A. and Rosolen, J.M. (2006) A multi-step treatment to effective purification of single-walled carbon nanotubes. *Carbon*, **44**, 3293–3301.
- 114** Ziegler, K.J., Gu, Z., Peng, H., Flor, E.H., Hauge, R.H. and Smalley, R.E. (2005) Controlled oxidative cutting of single-walled carbon nanotubes. *Journal of the American Chemical Society*, **127**, 1541–1547.
- 115** Li, Q.W., Yan, H., Zhang, J. and Liu, Z.F. (2002) Defect location of individual single-walled carbon nanotubes with a thermal oxidation strategy. *The Journal of Physical Chemistry B*, **106**, 11085–11088.
- 116** Lu, K.L., Lago, L.M., Chen, Y.K., Green, M.L., Harris, P.J. and Tsang, S.C. (1996) Mechanical damage of carbon nanotubes by ultrasound. *Carbon*, **34**, 814–816.
- 117** Wang, Y., Wu, J. and Wei, F. (2003) A treatment to give separated multi-walled carbon nanotubes with high purity, high crystallization and a large aspect ratio. *Carbon*, **41**, 2939–2948.
- 118** Pierrard, N., Fonseca, A., Konya, Z., Willems, I., Van Tendeloo, G. and Nagy, J.B. (2001) Production of short carbon nanotubes with open tips by ball milling. *Chemical Physics Letters*, **335**, 1–8.
- 119** Boccaleri, E., Arrais, A., Frache, A., Giannelli, W., Fino, P. and Camino, G. (2006) Comprehensive spectral and instrumental approaches for the easy monitoring of features and purity of different carbon nanostructures for nanocomposite applications. *Materials Science and Engineering B*, **131**, 72–82.
- 120** Belin, T. and Epron, F. (2005) Characterization methods of carbon nanotubes: a review. *Materials Science and Engineering B*, **119**, 105–118.
- 121** Lafi, L., Cossement, D. and Chahine, R. (2005) Raman spectroscopy and nitrogen vapor adsorption for the study of structural changes during purification of single-wall carbon nanotubes. *Carbon*, **43**, 1347–1357.
- 122** Ferrari, A.C. and Robertson, J. (2000) Interpretation of Raman spectra of disordered and amorphous carbon. *Physical Review B-Condensed Matter*, **61**, 14095–14106.
- 123** Brown, S.D., Jorio, A., Dresselhaus, M.S. and Dresselhaus, G. (2001) Observations of D-band feature in the Raman spectra of carbon nanotubes. *Physical Review B-Condensed Matter*, **64**, 0734011–0734014.
- 124** Dresselhaus, M.S., Dresselhaus, G., Jorio, A., Souza Filho, A.G. and Saito, R. (2002) Raman spectroscopy on isolated single wall carbon nanotubes. *Carbon*, **40**, 2043–2061.
- 125** Dillon, A.C., Parilla, P.A., Alleman, J.L., Gennett, T., Jones, K.M. and Heben, M.J. (2005) Systematic inclusion of defects in pure carbon single-wall nanotubes and their effect on the Raman D-band. *Chemical Physics Letters*, **401**, 522–528.
- 126** Reznik, D. and Olk, C.H. (1995) X-ray powder diffraction from carbon

- nanotubes and, nanoparticles. *Physical Review B-Condensed Matter*, **52**, 116–124.
- 127** Kataura, H., Kumazawa, Y., Maniwa, Y., Umezū, I., Suzuki, S., Ohtsuka, Y. and Achiba, Y. (1999) Optical properties of single-wall carbon nanotubes. *Synthetic Metals*, **103**, 2555–2558.
- 128** Itkis, M.E., Perea, D.E., Niyoki, S., Rickard, S.M., Hamon, M.A., Hu, H., Zhao, B. and Haddon, R.C. (2003) Purity evaluation of as-prepared single-walled carbon nanotube soot by use of solution-phase near-IR spectroscopy. *Nano Letters*, **3**, 309–314.
- 129** Landi, B.J., Ruf, H.J., Evans, C.M., Cress, C.D. and Raffaele, R.P. (2005) Purity assessment of single-wall carbon nanotubes using, optical absorption spectroscopy. *The Journal of Physical Chemistry. B*, **109**, 9952–9965.
- 130** Ryabenko, A.G., Dorofeeva, T.V. and Zvereva, G.I. (2004) UV-VIS-NIR spectroscopy study of sensitivity of single-wall carbon nanotubes to chemical processing and Van-der-Waals SWNT/SWNT interaction. Verification of the SWNT content measurements by, absorption spectroscopy. *Carbon*, **42**, 1523–1535.
- 131** Itkis, M.E., Perea, D.E., Jung, R., Niyoki, S. and Haddon, R.C. (2005) Comparison of analytical techniques for purity evaluation of single-walled carbon nanotubes. *Journal of the American Chemical Society*, **127**, 3439–3448.
- 132** Harutyunyan, A.R., Pradhan, B.K., Chang, J., Chen, G. and Eklund, P.C. (2002) Purification of single-wall carbon nanotubes by selective, microwave heating of catalyst particles. *The Journal of Physical Chemistry. B*, **106**, 8671–8675.
- 133** Shi, Z., Lian, Y., Liao, F.H., Zhou, X., Gu, Z., Zhang, Y., Iijima, S., Li, H., Yue, K.T. and Zhang, S.L. (2000) Large scale synthesis of single-wall carbon nanotubes by arc-discharge method. *Journal of Physics and Chemistry of Solids*, **61**, 1031–1036.
- 134** Arepalli, S., Nikolaev, P., Gorelik, O., Hadjiev, V.G., Holmes, W., Files, B. and Yowell, L. (2004) Protocol for the characterization of single-wall carbon nanotube material quality. *Carbon*, **42**, 1783–1791.
- 135** Yakobson, B.I., Brabec, C.J. and Bernholc, J. (1996) Nanomechanics of carbon tubes: Instabilities beyond linear response. *Physical Review Letters*, **76**, 2511–2514.
- 136** Yakobson, B.I., Campbell, M.P., Brabec, C.J. and Bernholc, J. (1997) High strain rate fracture and C-chain unraveling in carbon nanotubes. *Computational Materials Science*, **8**, 341–348.
- 137** Iijima, S., Brabec, C., Maiti, A. and Bernholc, J. (1996) Structural flexibility of carbon nanotubes. *Journal of Chemical Physics*, **104**, 2089–2092.
- 138** Hernandez, E., Goze, C., Bernier, P. and Rubio, A. (1998) Elastic properties of C and B_xC_yN_z composite nanotubes. *Physical Review Letters*, **80**, 4502–4505.
- 139** Lu, J.P. (1997) Elastic properties of carbon nanotubes and nanoropes. *Physical Review Letters*, **79**, 1297–1300.
- 140** Natsuki, T., Tantrakarn, K. and Endo, M. (2004) Prediction of elastic properties for single-walled carbon nanotubes. *Carbon*, **45**, 39–45.
- 141** Falvo, M.R., Clary, G.J., Taylor, R.M. JII, Chi, V., Brooks, F.P. J Jr, Wasburn, S. and Superfine, R. (1997) Bending and buckling of carbon nanotubes under large strain. *Nature*, **389**, 582–584.
- 142** Treacy, M.M., Ebbesen, T.W. and Gibson, J.M. (1996) Exceptionally high Young's modulus observed for individual carbon nanotubes. *Nature*, **381**, 678–680.
- 143** Krishnan, A., Dujardin, E. and Ebbesen, T.W. (1998) Young's modulus of single-walled nanotubes. *Physical Review B-Condensed Matter*, **58**, 14013–14019.
- 144** Wong, E.W., Sheehan, P.E. and Lieber, C. (1997) Nanobeam mechanics: elasticity, strength and toughness of nanorods and nanotubes. *Science*, **277**, 1971–1975.
- 145** Salvétat, J.P., Kulik, A.J., Bonard, J.M., Briggs, A.D., Stockli, T., Metenier, K.,

- Bonnamy, S., Beguin, F., Burnham, N.A. and Forro, L. (1999) Elastic modulus of ordered and disordered multi-walled carbon nanotubes. *Advanced Materials*, **11**, 161–165.
- 146 Yu, M.F., Lourie, O., Dyer, M.J., Kelly, T.F. and Ruoff, S. (2000) Strength and breaking mechanism of multi-walled carbon nanotubes under tensile load. *Science*, **287**, 637–541.
- 147 Yu, M.F., Files, B.S., Arepalli, S. and Ruoff, S. (2000) Tensile loading of ropes of single wall carbon nanotubes and their mechanical properties. *Physical Review Letters*, **84**, 5552–5555.
- 148 Xie, S., Li, W., Pan, Z., Chang, B. and Sun, L. (2000) Mechanical and physical properties on carbon nanotube. *Journal of Physics and Chemistry of Solids*, **61**, 1153–1158.
- 149 Demczyk, B.G., Wang, Y.M., Cumings, J., Hetman, M., Han, W., Zettl, A. and Ritchie, R.O. (2002) Direct mechanical measurement of the tensile strength and elastic modulus of multiwalled carbon nanotubes. *Materials Science and Engineering A*, **334**, 173–178.
- 150 Dereli, G. and Ozdogan, C. (2003) Structural stability and energetics of single-walled carbon nanotubes under uniaxial strain. *Physical Review B-Condensed Matter*, **67**, 0354161–0354166.
- 151 Huang, J.Y., Chen, S., Wang, Z.Q., Kempa, K., Wang, Y.M., Jo, S.H., Chen, G., Dresselhaus, M.S. and Ren, Z.F. (2006) Superplastic carbon nanotubes. *Nature*, **439**, 281–281.
- 152 Jacobsen, R.L., Tritt, T.M., Guth, J.R., Ehrich, A.C. and Gillespie, D.J. (1995) Mechanical properties of vapor-grown carbon fiber. *Carbon*, **33**, 1217–1221.
- 153 Ishioka, M., Okada, T. and Matsubara, K. (1992) Mechanical properties of vapor-grown carbon fibers prepared from benzene in Linz-Donawitz converter gas by floating catalyst method. *Journal of Materials Research*, **7**, 3019–3022.
- 154 Ghosh, S., Calizo, I., Teweldebrhan, D., Pokatilov, E.P., Nika, D.L., Balandin, A.A., Bao, W., Miao, F. and Lau, C.N. (2008) Extremely high thermal conductivity of graphene: Prospects for thermal management applications in nanoelectronic circuits. *Applied Physics Letters*, **92**, 1519111–1519113.
- 155 Bokros, J.C. (1969) Deposition, structure and properties of pyrolytic carbon, in *Chemistry and Physics of Carbon*, vol. 5 (eds L. S. Philip and J.R. S Walker), Marcel Dekker, New York, USA, pp. 97–103.
- 156 Buechler, R.A. (1944) Thermal and electrical conductivity of graphite and carbon at low temperatures. *Journal of Applied Physics*, **15**, 452–454.
- 157 Berber, S., Kwon, Y.K. and Tomanek, D. (2000) Unusually high thermal conductivity of carbon nanotubes. *Physical Review Letters*, **84**, 4613–4616.
- 158 Xiao, Y., Yan, X.H., Cao, J.X. and Ding, J.W. (2003) Three-phonon Umklapp process in zigzag single-walled carbon nanotubes. *Journal of Physics: Condensed Matter*, **15**, L341–L347.
- 159 Cao, J.X., Yan, X.H., Xiao, Y. and Ding, J.W. (2004) Thermal conductivity of zigzag single-walled carbon nanotubes: Role of the umklapp process. *Physical Review B-Condensed Matter*, **69**, 0734071–0734074.
- 160 Yi, W., Lu, L., Zhang, D.L., Pan, Z.W. and Xie, S.S. (1999) Linear specific heat of carbon nanotubes. *Physical Review B-Condensed Matter*, **59**, R9015–R9018.
- 161 Kim, P., Shi, L., Majumdar, A. and McEuen, P.L. (2001) Thermal transport measurements of individual multiwalled nanotubes. *Physical Review Letters*, **87**, 2155021–2155024.
- 162 Hone, J., Whitney, M., Piskoti, C. and Zettl, A. (1999) Thermal conductivity of single-walled nanotubes. *Physical Review B-Condensed Matter*, **59**, R2514–R2516.
- 163 Zhang, H.L., Li, J.F., Yao, K.F. and Chen, L.D. (2005) Spark plasma sintering and thermal conductivity of carbon nanotube bulk materials. *Journal of Applied Physics*, **97**, 1143101–1143106.
- 164 Qin, C., Shi, X., Bai, S.Q., Chen, L.D. and Wang, L.J. (2006) High temperature

- electrical and thermal properties of the, bulk carbon nanotube prepared by SPS. *Materials Science and Engineering A*, **420**, 208–211.
- 165** Krishnan, K.S. and Ganguli, N. (1939) Large anisotropy of the electrical conductivity of graphite. *Nature*, **144**, 667.
- 166** Frank, S., Poncharal, P., Wang, Z.L. and de Heer, W.A. (1998) Carbon nanotube quantum resistors. *Science*, **280**, 1744–1746.
- 167** Wei, B.Q., Vajtai, R. and Ajayan, P.M. (2001) Reliability and current carrying capacity of carbon nanotubes. *Applied Physics Letters*, **79**, 1172–1174.
- 168** Ebbesen, T.W., Lezec, H.J., Hiura, J., Bennett, J.W., Ghaemi, H.F. and Thio, T. (1996) Electrical conductivity of individual carbon nanotubes. *Nature*, **382**, 54–56.
- 169** Thess, A., Lee, R., Nikolaev, P., Dai, H., Petit, P., Robert, J., Xu, C., Lee, Y.H., Kim, S.G., Rinzler, A.G., Colbert, D.T., Cuseria, G.E., Tomanek, D., Fischer, J.E. and Smalley, R.E. (1996) Crystalline ropes of metallic carbon nanotubes. *Science*, **273**, 483–487.
- 170** Fischer, J.E., Dai, H., Thess, A., Lee, R., Hanjani, N.M., Dehaas, D.L. and Smalley, R.E. (1997) metallic resistivity in crystalline ropes of single-wall carbon nanotubes. *Physical Review B-Condensed Matter*, **55**, R4921–R4924.
- 171** Sanvito, S., Kwon, Y.K., Tomanek, D. and Lambert, C.L. (2000) Fractional quantum conductance in carbon nanotubes. *Physical Review Letters*, **84**, 1974–1977.
- 172** Urbina, A., Echeverria, I., Perez-Garrido, A., Diaz-Sanchez, A. and Abellan, J. (2003) Quantum conductance steps in solutions of multiwalled carbon nanotubes. *Physical Review Letters*, **90**, 1066031–1066034.
- 173** Choi, W.B., Jin, Y.W., Kim, H.Y., Lee, S.J., Yun, M.J., Kang, J.H., Choi, Y.S., Park, N. S., Lee, N.S. and Kim, J.M. (2001) Electrophoresis deposition of carbon nanotubes for triode-type field emission display. *Applied Physics Letters*, **78**, 1547–1549.
- 174** Robertson, J. (2004) Realistic applications of CNTs. *Materials Today*, **7**, 46–52.
- 175** <http://www.nanoamor.com/>.